Journal of Power Sources 253 (2014) 150–166

Contents lists available at ScienceDirect

Journal of Power Sources

journal homepage: www.elsevier.com/locate/jpowsour

Review

Application of carbon materials in redox flow batteries

M.H. Chakrabarti [a,b,*], N.P. Brandon [c], S.A. Hajimolana [a], F. Tariq [c], V. Yufit [c], M.A. Hashim [a], M.A. Hussain [a], C.T.J. Low [d], P.V. Aravind [e]

[a] Department of Chemical Engineering, Faculty of Engineering, University of Malaya, Kuala Lumpur 50603, Malaysia
[b] Energy Futures Lab, Electrical Engineering Building, Imperial College London, South Kensington, London SW7 2AZ, UK
[c] Department of Earth Science and Engineering, Imperial College London, South Kensington, London SW7 2AZ, UK
[d] Electrochemical Engineering Laboratory, Energy Technology Research Group, Faculty of Engineering and the Environment, University of Southampton, Highfield, Southampton SO17 1BJ, UK
[e] Process and Energy Department, Delft University of Technology, Leeghwaterstraat 44, CA Delft 2628, The Netherlands

HIGHLIGHTS

- A comprehensive coverage on carbon materials used in redox flow batteries is given.
- The influence of nanotechnology and graphene is discussed in detail.
- The importance of studying RFB degradation mechanisms is emphasised.

ARTICLE INFO

Article history:
Received 24 September 2013
Received in revised form
7 December 2013
Accepted 9 December 2013
Available online 3 January 2014

Keywords:
Redox flow battery
Carbon-based electrodes
Nanotechnology
Graphene
X-ray tomography

ABSTRACT

The redox flow battery (RFB) has been the subject of state-of-the-art research by several groups around the world. Most work commonly involves the application of various low-cost carbon-polymer composites, carbon felts, cloth, paper and their different variations for the electrode materials of the RFB. Usually, the carbon-polymer composite electrode has relatively high bulk resistivity and can be easily corroded when the polarised potential on the anode is more positive than that of oxygen evolution and this kind of heterogeneous corrosion may lead to battery failure due to electrolyte leakage. Therefore, carbon electrodes with high electrical conductivity, acid-resistance and electrochemical stability are highly desirable. This review discusses such issues in depth and presents an overview on future research directions that may help commercialise RFB technology. A comprehensive discussion is provided on the advances made using nanotechnology and it is envisaged that if this is combined with ionic liquid technology, major advantages could be realised. In addition the identification of RFB failure mechanisms by means of X-ray computed nano tomography is expected to bring added benefits to the technology.

1. Introduction

The redox flow battery (RFB) has been reviewed comprehensively several times recently [1–8] giving in depth information about its redox chemistries (involving various different redox couples) as well as perspectives about future research directions. The RFB (a schematic is shown in Fig. 1 [9]), unlike other forms of electrochemical storage, is characterised by the ability to de-couple power and energy, allowing significant cost savings as energy requirements increase, and offering the potential for MW/MW-h scale storage. When the capability to pump anions and cations between electrodes is coalesced with ultra-high surface area carbons, it may be possible to produce low-cost batteries that can offer 320 km of travel in electric vehicles and be charged in times equivalent to that taken to refuel with gasoline [10]. A summary of carbon materials used in various different RFBs is provided in Table 1 [6].

Among the RFBs, the all-vanadium, zinc/bromine, iron/chromium and polysulphide/bromide (PSB) systems have been demonstrated at a few hundreds of kW and even at multi-MW levels [22]. Only the all-vanadium redox flow battery (VRB), however, has seen commercial testing in many countries including China, Canada [2] and Japan [3,4].

* Corresponding author. Department of Chemical Engineering, Faculty of Engineering, University of Malaya, Kuala Lumpur 50603, Malaysia. Tel.: +60 3 7967 7655; fax: +60 3 7967 5319.
E-mail addresses: mohammedharun77@yahoo.com, harun_chakrabarti@hotmail.com (M.H. Chakrabarti).

0378-7753/$ – see front matter © 2013 Elsevier B.V. All rights reserved.
http://dx.doi.org/10.1016/j.jpowsour.2013.12.038

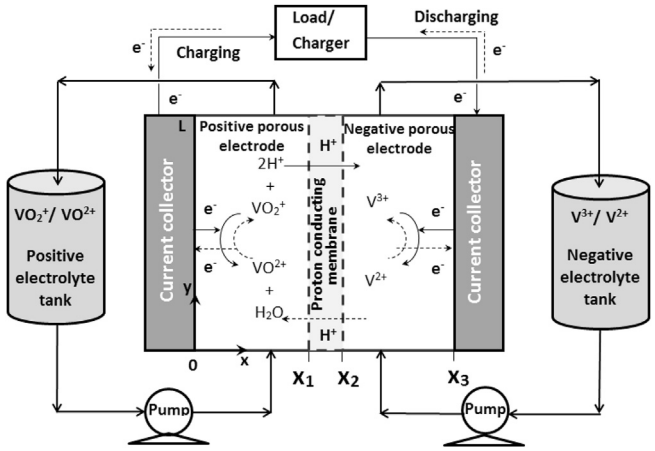

Fig. 1. A schematic representation of the most popular RFB system undergoing research to date (all-vanadium). The figure has been adapted from Ref. [9], copyright Elsevier.

Cost must still be further reduced for the complete commercialisation of VRB systems. According to the capital cost sensitivity analysis made by Zhang and co-workers [23], the cell stack is one of the highest cost components (this accounts for 31% of capital cost from a base case VRB). An effective solution to decreasing the stack cost is to increase the power density of a VRB during the charging–discharging process, thus limiting the size of the cell stack [24]. In order to achieve high power density and efficiency, a battery should be able to operate at a high voltage when discharging at ultra-high current densities (i.e., over 800 mA cm^{-2}). Various polarisation losses (activation, ohmic and concentration) have to be minimised, however, to maintain acceptable efficiency. Since both activation and concentration polarisations occur in the carbon-based electrode, the optimisation of this electrode configuration becomes a key point for cutting the cost of a VRB, and hence, any RFB system [25].

The compression and distortion of carbon felt electrodes inside an operating VRB rely on several parameters, such as the elastic modulus and thickness, clamping force, the pressures of the redox electrolyte flows, gasket material and thickness, temperature, humidity and many other factors [26]. The distortion of those materials contributes significantly to the efficiency of the flow-cell assembly and stack. If the clamping force is awkwardly small or big, the system efficiency is decreased [27]. After being clamped together in a RFB system, the carbon felt functions as a liquid diffusion layer, which may be one of the components with the most deformation [26]. The alteration of permeability or the pore size will definitely influence the power density or efficiency of the battery [28].

Considering the significant influence of carbon-based electrodes on the performance of RFBs, it is the need of the hour to review this topic in sufficient detail. Not only is an overview of technological development necessary but also a critical discussion on the influence of nanotechnology on the science is a significant requirement. In addition, it is paramount that suitable techniques are identified to ascertain battery degradation mechanisms at the nano-scale of carbon-based electrodes so that operating costs could be minimised. This paper aims to discuss such issues so that researchers may be stimulated to improve the design of carbon-based electrodes leading to the commercialisation of the RFB.

2. The influence of carbon-based electrodes on RFB design

The unique and competitive features of the VRB in comparison to other RFBs such as the iron/chromium system (ICB) are due to its long cycle life and high energy efficiencies [29]. As with all flow battery systems, efficiency is related to good stack design and operation. In the case of bipolar stacks, the innate existence of shunt currents can impact battery performance. This predominantly arises in large power stack arrangements where a number of individual cells is linked in series with mutual electrolyte manifolds. Unlike other types of RFBs such as the zinc–bromine battery (ZBB) in which corrosion and deposition may transpire at electrodes as a consequence of shunt currents, VRB systems only suffer from power loss in stack performance, which is one of the advantages of eliminating metal plating and running the system with the same species in both half cells. For decent energy efficiency and thermal management, however, shunt current minimisation is significant.

In order to diminish the effect of shunt current on stack efficiency and temperature, it is necessary to use channels with longer lengths and smaller cross-sectional areas [29]. The longer the channels and the smaller their cross-sectional areas are, however, the more pumping power will be necessary to circulate the electrolyte throughout the stack. As pumping systems are usually run by the battery itself, a trade-off between pumping power and shunt loss therefore needs to be considered in real RFB systems so that a maximum efficiency may be realised with an optimal flow-frame design.

Most VRB cell stacks are manufactured in a parallel-feed design, in which the cells are linked electrically in series and the electrolytes are pumped into all cells in parallel [30]. The uniformity of the single-cell operation is largely influenced by the circulation of the

Table 1
Carbon electrode materials used for RFB applications are summarised below. NG: not given. Adapted from Leung et al. [6], copyright RSC.

C material	Manufacturer	Thickness/mm	Electrode polarity	RFB system	Ref.
CF GFA-type	SGL, Germany	8	Positive	Zinc/Cerium (Zn/Ce)	[11]
C-polymer: PVA, PVDF, HDPE	Entegris, USA	6	Negative	Zn/Ce	[11,12]
GF	Le Carbonne, France	NG	Positive and negative	All-vanadium	[13]
PAN-based GF	XinXing, China	5	Positive	Polysulphide/Bromide	[14,15]
Cobalt coated PAN-based GF	XinXing, China	5	Negative	Polysulphide/Bromide	[15]
RVC	ERG, USA	1.5	Positive	Flowing lead acid	[16]
GF bonded electrode assembly with non-conducting plastic substrate	FMI, USA	NG	Positive and negative	All-vanadium	[17]
C paper	SGL, Germany	0.41	Positive and negative	All-vanadium	[18]
Porous G	Union Carbide, USA	2	Positive and negative	Zinc/chlorine	[19]
CF	Fibre Materials, USA	2.8	Positive and negative	Zinc/Bromine	[20]
Cylindrical bed of C particles	Sutcliffe Speakman, UK	2.5	Positive and negative	Polysulphide/Bromide	[21]

CF = carbon felt; GFA = graphite soft felt application (manufactured by SGL); GF = graphite felt; RVC = reticulated vitreous carbon; PVA = polyvinyl acetate; PVDF = polyvinylidene-difluoride; HDPE = high density polyethylene.

electrolyte. The flow field is a crucial factor in the design of a cell stack. It determines the uniformity of the electrolyte in the carbon-based electrode and even directly influences the uniformity of the current density. Excessive local current density is a key contributor to stack performance decline. Therefore, elucidating the distribution of electrolyte velocity in the electrode and the location of excessive local current density is important when optimising the construction of the flow field to enhance the uniformity of the current density. In spite of this fact, little research is emphasised on this issue to date.

Research on other RFB systems also gave evidence of the influence of carbon-based electrodes on battery performance efficiency. For example, early work on ICB discovered that typical carbon felts (CFs) could sustain current densities of at least 1000 A ft^{-2} but at a great disadvantage to pumping power and cell voltage [31–33]. Pumping power experiments with varying cell configurations showed that a large percentage of the pumping power was ascribable to the CF electrode. Hence modified felt or non-felt type C (carbon) electrodes were suggested to reduce this problem [5].

It has been suggested that felt strands of various diameters or rigidity (of the precursor fibres) should be blended to harvest CF electrodes of required characteristics [31–33]. An alternative solution is to craft out a bipolar plate with an engineered, catalysed surface structure fabricated from a multitude of small dimples or truncated pyramids. Also "carbated" bipolar plates (0.9 mm) can diminish contact resistance between felt structures.

The importance of carbon-based electrodes can be ascertained from this section. Therefore a detailed consideration of the research conducted so far on their employment in RFBs is given below. This is followed by a discussion on the application of nanotechnology to improve carbon-based electrodes for potential commercial opportunities in the future.

3. Employment of carbon in various RFB configurations

As shown in Table 2, the electrode material has a large influence on the redox reactions of both V^{3+}/V^{2+} and VO_2^+/VO^{2+} (the active ions in a VRB) [30]. Therefore, a large amount of research has been carried out on the exploration and modification of carbon electrode materials.

VRB electrodes may be divided into two types, metal and carbon materials. A range of metal electrode materials such as lead, gold, platinum, platinised titanium (Pt–Ti), and iridium oxide dimensionally stable electrodes (DSAs) has been investigated for VRBs [30]. It has been found that the electrochemical reversibility for the VO_2^+/VO^{2+} redox couple is not significant on the gold electrode, while the lead and titanium electrodes are simply passivated in the potential range where the VO_2^+/VO^{2+} redox couple reactions occur.

Table 2
Standard rate constants (k_0) and diffusion constants (D) of V^{3+}/V^{2+} and VO_2^+/VO^{2+} reactions on various electrodes [30] (with permission from ACS).

Redox couple	k_0 (cm s^{-1})	D (cm^2 s^{-1})	Electrode
V^{3+}/V^{2+}	1.7×10^{-5}	1.41×10^{-6}	GC (glassy carbon)
V^{3+}/V^{2+}	5.5×10^{-4}	4.0×10^{-6}	PG (pyrolytic graphite or PG in the c-plane)
V^{3+}/V^{2+}	5.3×10^{-4}	2.4×10^{-6}	PFC (plastic formed carbon)
V^{3+}/V^{2+}	1.1×10^{-3}	4.0×10^{-6}	CP (carbon paper)
VO_2^+/VO^{2+}	7.5×10^{-4}	1.4×10^{-6}	GC
VO_2^+/VO^{2+}	1.3×10^{-4}	2.4×10^{-6}	PG (c-plane)
VO_2^+/VO^{2+}	8.5×10^{-4}	3.9×10^{-6}	PFC
VO_2^+/VO^{2+}	1.0×10^{-3}	2.4×10^{-6}	CP

k_0 = heterogeneous electrode rate constant; D = diffusion coefficient of electroactive species (in this case vanadium).

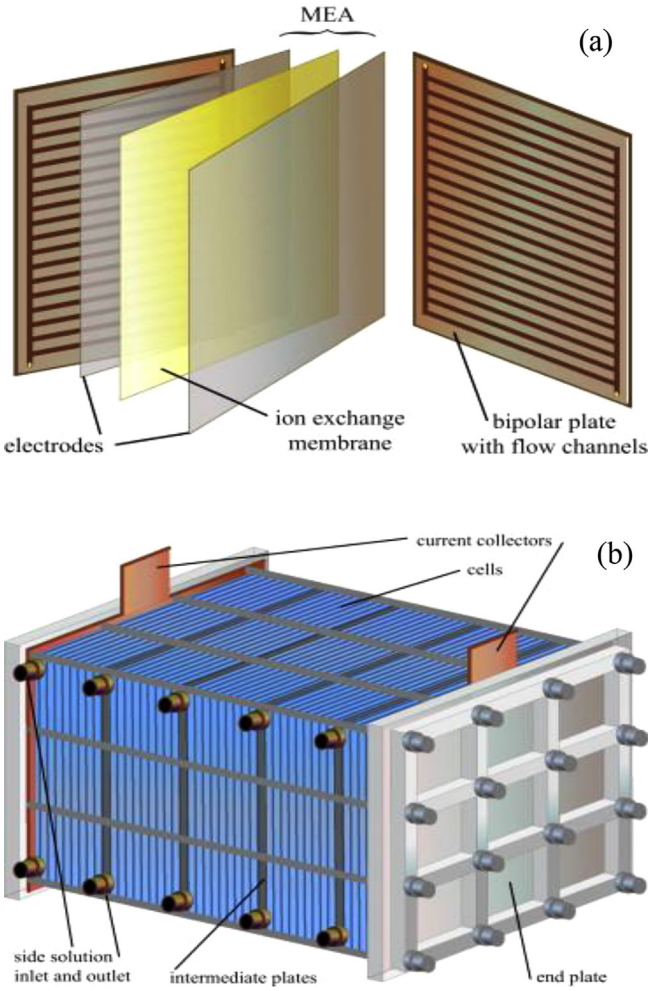

Fig. 2. (a) Diagram of a RFB cell with MEA (membrane-electrode assembly) elements and bipolar plates with parallel-channel layout for flow-by distribution;(b) RFB stacks with side fluid feedings—series of about 100 cells with active areas as large as 0.4 × 0.4 m are usual [4] (with permission from Elsevier).

This ultimately leads to an increase in cell electric resistance. The problem of the passivation film is successfully avoided if Pt–Ti and DSA are employed as electrodes; however, their high costs limit them from widespread use.

Carbon is an ideal VRB electrode material due to its wide operating potential range, high chemical stability and reasonable cost [30]. Several carbon materials such as carbon felt, graphite felt, carbon paper and graphite powder have been investigated as the electrodes for VRBs. Among them, carbon felt and graphite felt are preferred because of their enhanced three-dimensional network structures and higher specific surface areas, as well as good conductivity and chemical and electrochemical stability [34].

In addition, it has been discovered that several surface treatments may improve reaction kinetics on carbon electrodes. Chemical etching [35], thermal treatment [33], chemical doping [5], carbon nanotube (CNT) addition and doping of metallic catalysts onto the carbon fibres [36] have all been reported.

Typical cell stacks for RFBs consist of carbon materials as electrodes and bipolar plates (as shown in Fig. 2). Over the last two decades, several forms of graphite or vitreous carbon materials (including two- and three-dimensional electrodes) have been widely investigated in RFBs [6,37–41]. Some standard examples include graphite or carbon felts, carbon fibre, carbon cloth, carbon paper, thermal, hydroxylated and acid treated graphite and carbon-

polymer composite materials, carbon nanotubes (CNTs), iridium-modified (Ir-modified) carbon felt and graphene oxide (GNO) nanoplatelets [5,13,18,42–47]. Porous carbons [48] are also employed as electrode materials due to their high surface areas, good electrical conductivity and relative inertness. Such materials are available in diverse forms, ranging from isolated particles to monolithic foam and felt structures [49]. As pure carbon and graphite are brittle and usually difficult to scale-up in stacks, composites of polymer binders and conductive particles, such as carbon-polymer composites [50,51] and polymer-impregnated graphite plates [52,53] are usually employed, which possess advantages of low cost, light weight and good mechanical properties [6]. These are used in various systems, such as ZBB [52–54], VRB [17], PSB [15,55], zinc/cerium (Zn/Ce) [11,12,56] and soluble flowing lead/acid (Pb/H_2SO_4)RFBs [16,57].

Although a series of carbon and graphite felt materials is commonly available for use in RFBs with high energy efficiencies at current density ranges of up to 100 mA cm^{-2}, further enhancements in electrode activity may allow performance at better current densities. The resultant increases in stack power density may cause a reduction in electrode areas and stack sizes, allowing significant decreases in stack costs per kW of power output [2]. Efforts to improve effective surface area and electro-activity of carbon-based electrodes are presently underway in China and other parts of the world [35,37,58–61] and new composite electrode materials are also expected to emerge in the future [2]. The following subsections provide a detailed overview on various carbon- and graphite-based electrodes and electro-catalysts studied over the years in RFBs.

3.1. Carbon polymer

When AC/polyolefin (AC stands for activated carbon) composite electrodes were employed in the PSB system, the potential increased from 1.7 to 2.1 V during the charging process due to adsorption of Br (bromine) in the AC [62]. Zhong and co-workers [51] produced conducting polyethylene (PE) composite electrodes with low resistivities by mingling the polymer with conducting fillers (carbon black, graphite power and fibre) [41]. The chemical treatment of graphite fibre-based composite polymer electrodes with chromate-H_2SO_4 enhanced the surface and improved electrode reactions [63]. Carbon-polypropylene (C-PP) composite electrodes modified with rubber gave enhanced mechanical properties, lower permeability and improved overall conductivity in comparison to the PE composite electrodes [64,65]. A VRB attained a high voltage efficiency of 91% when it used the C-PP composites as its functioning electrode materials.

With regard to the bipolar electrode substrate, many groups have been developing carbon-filled polyolefin composite materials ("conducting plastics") that result in low cost, light weight, flexibility and ease of handling [64,65]. For such materials to result in good conductivity at high currents, however, the carbon felt has to be heat bonded to the "conducting plastic" to enable penetration of the carbon fibres through the surface to establish contact with the carbon filler inside the substrate. Although these heat bonded bipolar electrodes perform well under normal operating conditions, long-term overcharge can cause delamination and increased electrode resistance. Good cell potential control is therefore paramount to avoid damage to the bipolar electrodes [2].

Carbon-polymer composite materials may be held together by polymer binders, such as PVDF, HDPE [12], PVA [56] and polyolefin [66] by injection moulding, which is a low-cost method for producing large quantities easily [6]. A polymer-impregnated graphite plate may be manufactured by performing compression moulding on the expanded graphite with thermoplastic polymers. Since this moulding technique permits the use of a higher proportion of graphite than the injection moulding procedure, it has better electrical conductivity. Due to the thermoplastic properties of the polymer employed in this method, the mechanical properties, chemical resistance and thermal stability are improved in comparison to those produced by injection moulding. Since a longer time is necessary to cool down the mould before each half plate can be removed, the production cycle can be quite time consuming (typically in the range of 10 min). Therefore, the higher costs of this procedure could hinder its use in RFBs for large-scale applications [67,68]. Conductivity of the aforementioned composite materials may be achieved by adding conductive filler material [17] or AC particles [36,69].

Currently, the materials used in VRBs include polymer-impregnated graphite plates, conductive carbon-polymer composites [50,51] and polymer-impregnated flexible graphite [52,53]. The polymer-impregnated graphite plate is widely used because of its low electronic resistance and ease of production [22]; however, its relatively high cost and brittleness may have limited its practical use. Conductive carbon-polymer composites, in contrast, have become an attractive alternative for the VRB bipolar plates in recent years due to its low cost, light weight properties and flexibility [50,51,64,65,70,71].

3.2. CF

One of the key components in RFBs (especially for VRBs) is carbon felt (CF), which performs as the liquid diffusion layer (LDL) and differentiates distinctively from the gas diffusion layer (GDL) in proton exchange membrane fuel cells (PEMFCs) such that the thickness of the LDL is in the mm range, whereas the size of the GDL is about 1/5–1/10th of the PEMFC [26]. One reason for a significantly thick CF is due to the enhancement of diffusion lengths for VRB applications, which tends to minimise the associated resistance. While the thickness of the LDL plays the role of stress absorber and maintains the conductivity and the electrical contacts, the durability of the MEA is reasonably safeguarded.

Typical RFB CF electrode materials have a porosity around 0.8, a fibre diameter of approximately 10 μm and a permeability of 20×10^{-8} cm^2 [63]. A qualitative estimate of the surface area variation with fibre diameter can be determined using a filament equivalent model which involves estimating the number of cylinders N of a given diameter d_f that possess a specified porosity ε (cm^3/cm^3), then calculating the specific surface area $a_{1,2}$ (cm^2/cm^3) of N cylinders. A simple formula for this relationship is described by Carta and co-workers as [72]

$$a_{1,2} = 4 \times (1 - \varepsilon)/d_f$$

Two-dimensional CF electrodes were reported to be chemically unstable for the redox reactions of VO_2^+/VO^{2+}(the positive redox couple of a VRB) [21,73–77] and Ce^{3+}/Ce^{4+}(the positive redox couple of the Zn/Ce flow battery) [11,78] due to the evolution of CO_2 [79]. Since these reactions occurred at highly positive potentials and the local current density at the planar electrode surface underneath the CF was very high, physical deterioration of the electrode surface was observed [6]. It was found, however, that by mechanically compressing the CF onto the carbon-based current collector used in the positive electrode, the VRB and the Zn/Ce systems operated at a projected current density of 0.5 mA cm^{-2} with a voltage efficiency of over 75% [11,75].

Some researchers further improved the catalytic properties and the conductivity of CFs by depositing metals on the electrode surface [43,80]. For instance, Sun and Skyllas-Kazacos [80] modified CF electrodes through impregnation with ions such as Pt^{4+}, Au^{4+}, Ir^{3+} and several others [6]. In terms of the electrocatalytic activity and

stability, a modified Ir^{3+} electrode was discovered to give the best performance when it was used as the positive electrode in a VRB. In another study, Fabjan and co-workers [81] reported that Ru oxide (RuO_2) improved the reaction rate and decreased the side reactions such as gaseous evolution. More recently, non-precious Bi [82] and manganese oxide (Mn_3O_4) [83] were also found to improve electrocatalytic activity after modification of the CF [6].

A recent study describes a new Ni plated CF and the effect of plating thickness on mechanical, electrical and morphological properties [26]. Experimental results show that the nickel coated CF prepared by electro-less plating is successfully applied and a drastically reduced area specific resistance of 50% can be obtained under 40% compression, while the stress–strain curve, residual strain and porosity basically remain unchanged. The nickel coated CF appears to be a promising electrode material for VRB applications. Future work involves applying these plated CFs to the actual VRB and the investigation of the relation of enhanced conductivity and the electrical contacts.

3.3. GF

Novel modifications of graphite felt (GF) materials were carried out by numerous researchers (especially for the VRB system) [84–88]. For instance, the GF was modified by treating it with H_2SO_4 followed by heat treatment [73,74,80]. During the acid treatment, surface functional groups, such as −C=O and −COOH, were formed on the electrode surface, which was found to significantly increase the chemical activity in the highly acidic media [6]. Further details are provided in the following paragraphs.

Despite the fact that GFs have a wide operating potential range, good stability and low cost, they are plagued with serious disadvantages such as low surface area and electrocatalytic activity (poor kinetics and reversibility). Therefore, it is of critical importance to develop GF materials with high electrocatalytic activity towards the redox reactions in the VRB system [89]. To address this issue, various approaches including heat treatment, acidic oxidation and modification with metals have been pursued by several research groups [42,60,82,88,90–94].

Sun and Skyllas-Kazacos [73] employed heat treatment at 400 °C for 30 h to improve the electrochemical activity of GFs. An improvement in energy efficiency of VRBs from 78 to 88% was reported [22]. The increased activity was ascribed to the improved surface hydrophilicity and the formation of the functional groups of C–O–H and C=O on the surface of the GF. The authors suggested that the C–O groups on the electrode surface behaved as active sites and catalysed the reactions of the vanadium species. Despite that, it was found that a strongly acidic carboxyl group was formed at room temperature after the carbon was treated with sodium hypochlorite, potassium permanganate or ammonium persulfate solutions [22]. Sun and Skyllas-Kazacos [74] investigated the electrochemical properties of the GF after it was treated with concentrated H_2SO_4 or HNO_3. A significant improvement in both coulombic and voltage efficiencies of the VRB was achieved with GF treated by means of concentrated H_2SO_4. The improved activity of the VRB was once again ascribed to the increased concentrations of surface functional groups that formed during acidic treatment [22] as in the case for thermal treatment [73]. These functional groups not only led to an increase in the hydrophilicity of the GF but also behaved as active sites for the electrochemical reactions [22].

Another method involved a combination of chemical and thermal treatments of GF. The GF was treated initially in 98 wt.% H_2SO_4 for 5 h and then kept at 450 °C for 2 h [22]. The synergistic effects of acid and heat from the process increased the −COOH functional groups on the GF surface and its surface area from 0.31 to 0.45 $m^2\ g^{-1}$. As a result, the electrode activity was significantly improved, which was mainly accredited to the increase of the −COOH groups that behaved as active sites, catalysing the reactions of the vanadium species and accelerating both electron and O_2 transfer processes [1,2,22].

Electrochemical oxidation was employed recently to modify the GFs to improve their activity towards the electrochemical reactions between vanadium species in VRBs [22]. Li et al. [58,95] investigated the characteristics of GF oxidised electrochemically for VRBs while Tan et al. [96] studied the activation mechanisms of electrochemically-treated GF. The studies indicated that −COOH functional groups formed on the GF surfaces, leading to both increased surface areas as well as O/C ratios [97]. AC impedance data showed a reduction in resistance to the reactions of the vanadium species. The mechanism of the improvement in the electrochemical activity of GF was accredited to the formation of a C–O–V bond, which enhanced the electron transfer for the reactions on both positive and negative electrodes and the O_2 transfer for the reactions on the positive electrode [22].

In recent years [22], the deposition of metals on the surface of GFs was used to significantly enhance their electrochemical performance, mainly through the improvement of electrical conductivity. The initial studies proposed metallization by impregnation or ion exchange with solutions containing Pt^{4+}, Au^{4+}, Ir^{3+} or other ions. The best electrocatalytic behaviour for vanadium redox couples in an H_2SO_4 solution was obtained using materials modified with Ir^{3+} [80]. Other studies investigated the distribution of metals (antimony, arsenic, selenium or iridium) or alloys (PtRu) on the surface of carbon materials after they had been subjected to different treatments such as thermal reduction [98] or electrode deposition. In the former case, the carbon material was immersed in a solution containing the metallic ions and then it was thermally treated in air at high temperatures. In the latter case, the metal was electrodeposited from a galvanic bath onto the surface of the carbon material through the application of an arbitrary current. In both cases the main objective was to reduce the concentration of metal on the surface of the electrodes [82].

González and co-workers [82] also performed separate investigations upon the electrochemical behaviour of a GF modified with thermally reduced Bi as positive electrode material in a VRB. Although this metal was successfully used to measure concentrations of trace metals [99–101], as an alternative to commonly employed toxic mercury, this was the first time that Bi was applied to the VRB. Additional advantages of the research carried out in the work included the low cost of Bi in comparison to other metals like Pt, Au or Ir as well as the low metal concentration requirement on the surface of the GF [82].

Several methods to produce vapour grown carbon fibres (VGCFs) on GF as electrodes for VRBs have been reported recently [102]. The experiments include GF preparation and VGCF production onto graphite fibre in the GF. Various attempts have been made using Ni and cobalt (Co) catalyst coatings on the GF. The Ni catalyst has come from nickel nitride solution. It has been prepared by dipping GF into the solution prior to thermal decomposition. Co nanoparticles have been sprayed onto the GF. Both experiments have resulted in the growth of CNTs and VGCFs onto graphite fibres in the GF. The experimental results have shown that VGCFs and CNTs with the size range of 20–70 nm in diameter have been grown in the GF using different catalysts. The encouraging results have also indicated that the single VRB cell using new electrodes can increase the charge/discharge efficiency by more than 12% in comparison to conventional GF electrodes.

3.4. PAN-based CF or GF

To date, the PAN-based GF is the most common electrode material used in the VRB [14,103]. The PAN-based GF has advantages of

a wide potential range, good electrochemical activity, high chemical stability and low cost [6].

Compared with the negative electrode, the kinetics of the VO_2^+/VO^{2+} redox reaction is significantly slower when rearranging the coordination structures of the vanadium ions, which consequently become the electrochemical rate limiting step [104] thereby affecting the energy efficiency. In spite of that, the conventional PAN-based CF electrode demonstrates poor kinetic reversibility [43], due to which, developing a promising electrode is imperative for a VRB system [103].

A novel method of hydrothermal ammoniated treatment of the PAN-based GF for the VRB has been reported recently [88]. The GF has been treated in a Teflon-lined stainless steel autoclave for different times at 180 °C. The content of nitrogen in the PAN GF has changed from 3.803 to 5.367 wt.% by adjusting the treatment time to 15 h in ammonia solution, while Fourier transformation infrared (FT-IR) results indicate that nitrogenous groups have been introduced [105]. The electrochemical properties of these GFs have been characterised by cyclic voltammetry (CV), electrochemical impedance spectroscopy (EIS) as well as cell charge and discharge tests [88]. The energy efficiency of the treated GF has reached 85% at a current density of 20 mA cm^{-2}. The corresponding coulombic and voltage efficiencies are 95.3% and 75.1%, respectively. The improvement of the electrochemical properties for the treated GF has been attributed to the increase in polar nitrogenous groups on the carbon fibre surface, which has facilitated charge transfer between the electrode and vanadium ions.

3.5. AC

AC particles are widely used as sorbents; in addition to a high surface area, the materials show a microporous structure, the ability to adsorb a wide spectrum of species and a high surface reactivity [69]. Such properties are exploited in electro-sorption experiments, where a bed of AC particles (or felt) under potentiostatic control is used to remove metallic ions or dissolved organic species [106–109]. AC particles have been intensively characterised in terms of their surface, pore size distribution and activity [110,111]. Electrodes for filter-press cells (including RFBs) can be manufactured from AC–polymer particles [69].

Fig. 3 illustrates the overall cell voltage of a mono-polar PSB with AC/polyolefin pressed electrodes divided by a Nafion® 115 membrane containing 5 mol dm^{-3} NaBr as anolyte and

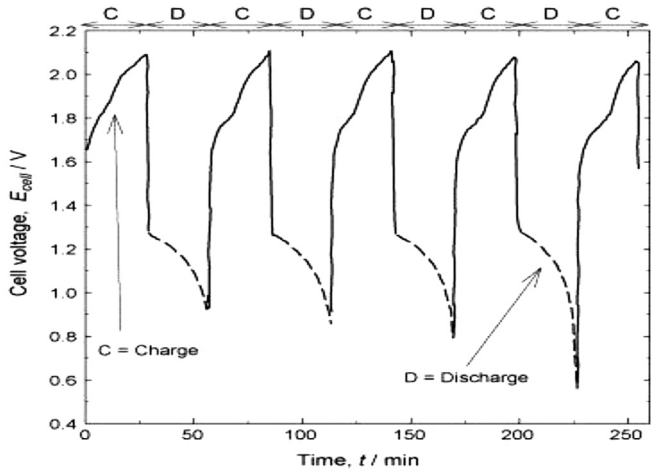

Fig. 3. Cell potential against time during charge/discharge cycles at a current density of 40 mA cm^{-2} for a PSB mono-polar test cell with AC-polyolefin pressed plates as electrode materials [1,6,66] (with permission from Elsevier).

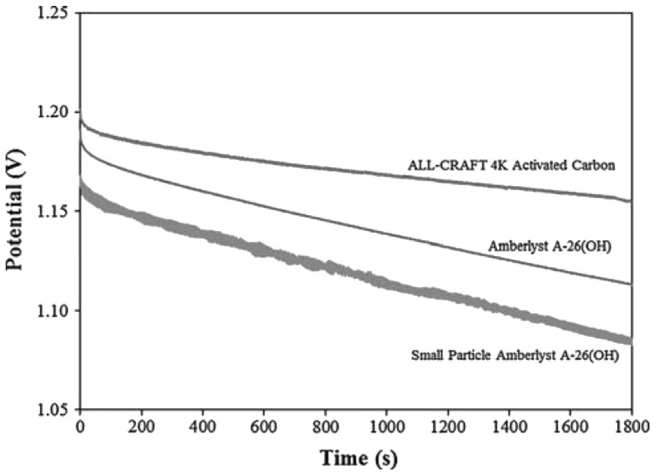

Fig. 4. Average potential profiles for a packed-bed electrode RFB with a range of separator materials. Taken from Sawyer and co-workers [113], with permission from Springer.

1.2 mol dm^{-3} Na_2S as a catholyte [66]. During the charging cycle for 30 min at 40 mA cm^{-2} the cell voltage climbs sharply from 1.7 to 2.1 V [6]. This behaviour is explained by the different overpotentials created within the cell and the adsorption of Br on the AC. During the discharge cycle at the same current, the plot shows a characteristic critical point at which the voltage drops, indicating complete discharge. AC adsorbs Br giving easily available reactants and the discharge process only becomes mass transport controlled at high reactant conversion levels. Operation of RFBs under deep discharge and high fractional conversion conditions demands improved mass transport of the electro-active species. Under these circumstances, high electrolyte flow velocity, effective turbulence promoters and roughened electrode surfaces become significant factors in attaining a satisfactory performance [2,6].

Radford and co-workers [69] successfully characterised AC particles for PSB applications by using a laboratory-scale thin-layer, shallow packed-bed electrode cell reactor. High surface area ACs were used in an effort to make up for the slow kinetics of the chemical-electrochemical reaction and to classify the essential factors affecting the operation of candidate electrode materials for RFBs. The reactor was employed as a tool for the selection of AC particles used as raw materials for planar, moulded C-polymer composite electrodes in a similar manner to work reported in earlier publications [6,112].

The particles were affixed to a circular section (area = *ca.* 0.80 cm^2) on the shallow packed bed of 2.5 mm thickness in the direction of electrolyte flow (mean linear flow velocity ≈ 6 mm s^{-1}) [69]. CV in de-aerated, 1 mol dm^{-3} H_2SO_4 at 295 K gave a specific capacitance in the range of 50–140 F g^{-1}. Linear sweep voltammetry and galvanostatic step investigations in an alkaline sodium polysulphide electrolyte (1.8 mol dm^{-3} $Na_2S_{2.11}$) gave marked differences amongst several types of ACs. Such differences were highlighted during the galvanostatic charge–discharge cycling of half-cell electrodes in the $Na_2S_{2.11}$ electrolyte.

In earlier investigations, the application of packed-bed carbon electrodes in a flow type Zn/alkaline/manganese dioxide battery was discussed [10]. It was determined that increasing the separation between the anode and cathode had a negative impact, raising electrolyte flow had a positive impact and the presence of an intensely basic ion exchange resin between the anode and cathode had a positive impact on the cell potential [113]. Based on these results, a recent study [114] investigated applications of other materials between the carbon electrodes, effect of inter-electrode distance as well as the influence of electrolyte flow direction

(anode-to-cathode, cathode-to-anode) on the battery performance. The cathode consisted of 30 wt.% manganese (IV) oxide (60–230 mesh, ≥99%), 35 wt.% G and 35 wt.% 4K-AC.

Based on the results of using acidic and basic ion exchange resins as separating materials in the RFB it was decided to scrutinise the use of an ALL-CRAFT-AC as the separating material in an RFB [113]. ACs were known to contain both acidic and basic reactive sites. ACs were used as catalyst supports in packed-bed reactors and thus were not expected to cause an issue when employed inside the packed-bed RFB.

A comparison of the RFB operation when employing the ALL-CRAFT-AC in comparison to the stock Amberlyst A-26(OH) as well as against a decreased particle size Amberlyst A-26(OH) is shown in Fig. 4 (where the Amberlyte and Amberlyst are liquid chromatography resin beads) [113]. The ALL-CRAFT 4K-AC operates better and a similar sized Amberlyst A-26(OH) gives worse performance than the stock Amberlyst A-26(OH), thereby ruling out particle size as a reason for the operational gain of the 4K-AC.

The RFB performance results suggest that the ALL-CRAFT 4K-AC improves system operation by displaying a greater basicity than the Amberlyst A-26(OH) [113]. The basicity may be innate in the material structure or it may be a result of electrolyte acceptance into the pores of the AC by means of absorption that behaves as an electrolyte reservoir. Both solid-phase surface area and ionic site density benefit the ability of solid materials in the separator to reduce ion-ohmic overpotentials [115]. The data in Fig. 4 are consistent with a solid-phase ion transport mechanism that is robust at high current densities.

3.6. RVC

Due to the large volumetric surface areas, typically 240–400 cm^2 cm^{-3} and 5–70 cm^2 cm^{-3} for the CF [116] and the RVC foam [117], respectively, three-dimensional carbon-based materials have been employed in various RFB systems [6]. RVC electrodes have also been employed in ZBB [117] and soluble Pb/H_2SO_4 RFBs [16]. The porosity of this material is useful in retaining the solid complex of bromide during charging of a ZBB system [118], while the rough surface of the scraped RVC in the soluble Pb/H_2SO_4 RFB allows sticky deposits to be formed within the compressed foam structure [16].

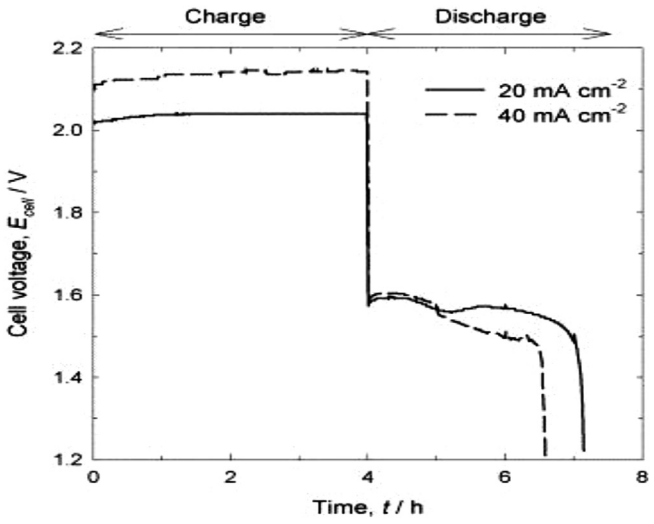

Fig. 5. RFB potential vs. time for a cell with RVC positive and negative electrodes separated by a 4 mm inter-electrode gap in 1.5 mol dm^{-3} $Pb(CH_3SO_3)_2$ + 0.9 mol dm^{-3} CH_3SO_3H + 1 g dm^{-3} Ni(II) + 1 g dm^{-3} Na ligninsulfonate [6,126] (with permission from Elsevier). Mean linear flow rate of 10 cm s^{-1} was employed.

The Pb/H_2SO_4 RFBs have been studied in several electrolytes; perchloric acid [119–121], HCl, hexafluorosilicic acid, tetrafluoroboric acid [122–125] and more recently in methanesulfonic acid (CH_3SO_3H) [16,126–128]. Fig. 5 illustrates the cell potential against time response during the charge/discharge cycles of a soluble Pb/H_2SO_4 RFB in CH_3SO_3H at two different current densities [126]. The experiments have been performed in an undivided RFB containing positive and negative electrodes made of 70 ppi RVC and 40 ppi reticulated Ni, respectively [6]. The RFB has a 4 mm inter-electrode gap and the electrodes have been prepared by pressing them onto a carbon powder/high density PE back plate current collector of an area of 2 cm^2. The electrolyte contains 1 g dm^{-3} of sodium ligninsulfonate as an additive to decrease the roughness of the Pb deposit thereby avoiding the formation of dendrites. This tends to improve the kinetics of the Pb(II)/PbO_2 couple. The plots in Fig. 5 display constant potential during charge and slow potential drop during discharge. The overpotential is higher when the applied current is 40 mA cm^{-2} in comparison to 20 mA cm^{-2}. The charge and energy efficiencies at a current density of 20 mA cm^{-2} are 79% and 60% while at 40 mA cm^{-2} they are 65% and 46%, respectively. The response of cell potential vs. time for two sets of 15 min charge/discharge experiments at 20 mA cm^{-2} is shown in Fig. 6. The low overpotentials seen during the second cycle of the charging process has been explained by the occurrence of insoluble Pb(II) remaining in the positive electrode during the reduction of PbO_2. During the 79–84th cycles the shape of the plot remains the same but lower overpotentials during the discharge process can be seen [1,2,6].

3.7. GF bonded electrode assembly with conducting plastic substrate

Some manufacturers are currently employing polymer-filled expanded graphite board products, however, these materials happen to be very fragile and more expensive than the "conducting plastic" composites [2]. As they tend to be cumbersome to handle in large sizes, some stack developers have preferred to design and manufacture smaller stacks with electrode areas less than 1000 cm^2 and output power less than 7 kW. Each scalable system integrates energy storage and power management in 175 kW

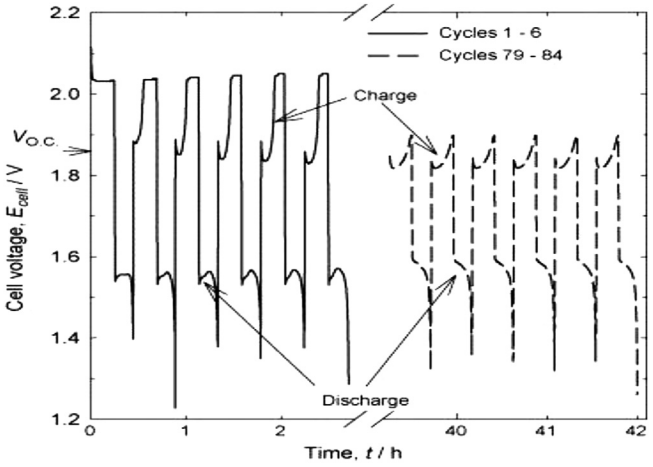

Fig. 6. Potential against time plots for 1–6 and 79–84 charge/discharge cycles at 20 mA cm^{-2} during 15 min charge of the soluble Pb/H_2SO_4 RFB. The cell consisted of a Ni foam negative electrode and an RVC positive electrode with 4 mm of inter-electrode gap in 1.5 mol dm^{-3} $Pb(CH_3SO_3)_2$ + 0.9 mol dm^{-3} CH_3SO_3H + 1 g dm^{-3} Ni(II) + 1 g dm^{-3} Na ligninsulfonate. Mean linear flow rate of electrolyte was 10 cm s^{-1}. Open circuit potential $V_{O.C.}$, shown in the figure, was 1.86 V [6]. Taken from Hazza et al. [126], copyright Elsevier.

modules of up to 10 MW of capacity and 60 MWh of storage. With a focus on MW-scale grid storage applications, however, scale-up to 50 kW stack sizes is important for ease of system assembly and integration [63].

Both Kashima-Kita Electric Power Corporation and Sumitomo Electric Industries (SEI) have successfully developed and tested 40–50 kW stacks with demonstrated overall energy efficiencies of 80% and cycle life as high as 270,000 in large-scale VRB field trials in Japan and elsewhere [2,129], while Innogy successfully designed a 100 kW stack for the Regenesys™ PSB (see Fig. 7). In each case, however, conducting plastic graphite composites have been used as the bipolar electrode substrate material, allowing large electrode areas to be employed. The development of novel and flexible, oxidation resistant bipolar electrode substrate materials therefore has allowed the production of large stacks that are resistant to overcharged conditions with greater ease of operation [2].

Vanadium–bromide (V/Br) systems have also used electrodes made of CF or GF bonded onto plastic or conductive plastic sheets [130,131]. A series of charge and discharge curves of the RFB at a current density of 20 mA cm^{-2} is displayed against time in Fig. 8. Generally, the coulombic efficiency increases with increasing current density due to lower self-discharge through the membrane; however, it decreases as temperature rises due to faster diffusion of vanadium and polybromide ions through the membrane [5].

3.8. Carbon plastic

Carbon plastic sheets were employed as current collectors in a VRB system as early as 1988 [50]. They were referred to as a graphite impregnated PE plates (0.26 mm thickness) and were heat bonded to GF electrodes. An overall energy efficiency of 84% was obtained at a charge and discharge current density of 30 mA cm^{-2} (charge/discharge curves are shown in Fig. 9). Other workers [81] also demonstrated similar performance for the VRB employing polyacrylonitrile (PAN) modified CF electrodes that were pyrolysed and heat-treated at 1900 °C prior to use. Later a Zn/Ce RFB system containing carbon plastic anodes and platinised Ti mesh cathodes of 100 cm^2 geometrical area separated by a (non-specified type of) Nafion® membrane was patented in 2004 [132].

3.9. Carbon or graphite cloth

The PSB system was tested with carbon cloth [15] but not in as much detail as for VRBs [13,30,77,81,97,133,134]. Details of cell testing for the VRB were provided by Kaneko and co-workers [77]. Two types of carbon cloth electrodes (GF-20, BW-309) were evaluated in depth. They were made from different carbon precursors (GF-20 PAN type and BW-309 cellulose type) but had similar surface structure. The electromotive force (EMF), current density and total energy efficiency of the small-scale cell of V-V-H_2SO_4 system were 1.4 V, 1.4 A cm^{-2} and 87.3%, respectively and these results were better than those obtained by Kazacos and Skyllas-Kazacos [50] earlier using thick GF electrodes.

Fig. 7. Interior view of Innogy's 12 MW Regenesys™ plant at Little Barford in the UK. Figure was reproduced with kind permission from the Department for Business, Innovation and Skills, Government of U.K. and the ECS [2].

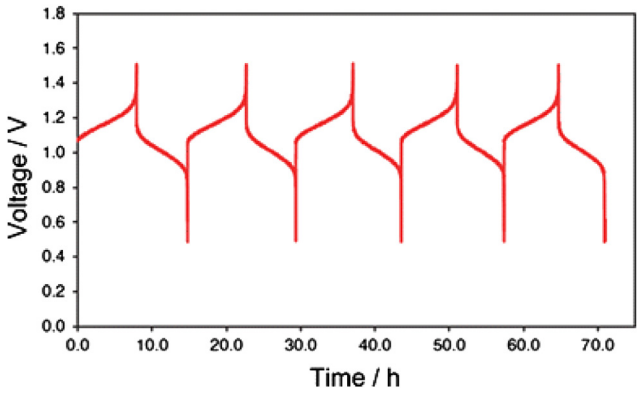

Fig. 8. Charging and discharging time against number of cycles for a 2.5 M V-bromide RFB using C material bonded to conductive plastic sheets separated by a Nafion® 112 cationic membrane. The charge/discharge current density was 20 mA cm^{-2} and the cell operated at 20 °C. Obtained from Weber et al. [5] with permission from Springer.

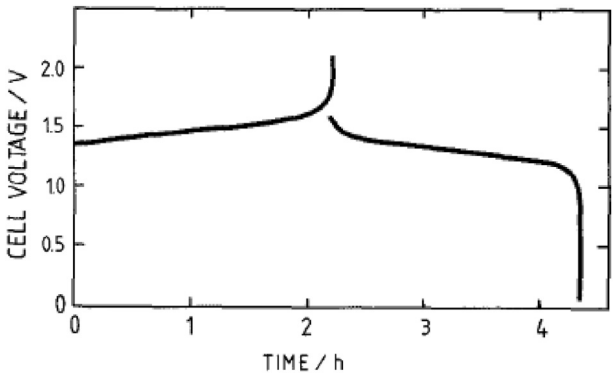

Fig. 9. Charge/discharge performance of carbon plastic electrodes in the VRB at 35 °C [50] (copyright ECS).

Matsuda and co-workers [135] also used carbon fibre cloth electrodes to evaluate the performance of an all-organic redox flow battery based on acetonitrile. For a single pass system, an overall energy efficiency of 18% was achieved. Recently, researchers in M.I.T. [136] have used a commercial carbon cloth gas diffusion anode with 0.5 mg cm^{-2} of platinum (60 wt.% supported on carbon) to operate a membrane-less hydrogen bromine laminar flow battery (HBLFB) with reversible reactions and a peak power density of 0.795 W cm^{-2} at room temperature and atmospheric pressure. The power density reported by the authors represented the highest value ever observed in a laminar flow electrochemical cell by a factor of three. Similar results were only observed by the University of Tennessee using carbon paper electrodes [137].

3.10. Carbon paper

To enhance the electrochemical performance of electrodes in the VRB, carbon paper electrode was treated with an H_2O_2 and

H_2SO_4 solution, according to the hydrothermal acid oxidation method, in a Teflon-lined stainless steel autoclave over varying time periods at 180 °C [137]. The water contact angle test showed that the contact angle of treated carbon paper samples changed from 120 to 100.8 °C by adjusting the treatment time from 6 to 18 h. Furthermore, a treatment time of 12 h resulted in the lowest contact angle observed, indicating that the wetting property of the carbon paper had been improved under these treatment conditions. FT-IR spectroscopy results showed that oxygen-containing groups, such as the carbonyl and carboxyl groups, had been successfully introduced to the carbon papers. Scanning electron microscopy (SEM), CV, EIS and charge–discharge tests were carried out to characterise the surface topography and electrochemical properties of the carbon papers. The treated samples displayed high activity for the redox reactions of V(IV)/V(V) or VO^{2+}/VO_2^+. A single-RFB employing carbon paper was applied for 12 h as an electrode and exhibited an excellent performance. The energy efficiency reached 80% at a current density of 30 mA cm^{-2}. The corresponding coulombic and voltage efficiencies were 96% and 84%, respectively [137].

Recently, a VRB with a peak power density of 557 mW cm^{-2} [18], which is over five-fold higher than that of other conventional published systems [50,138–140], has been demonstrated and reported by the University of Tennessee [141]. This high power density is obtained with a no-gap-serpentine architecture similar to fuel cells with carbon paper electrodes. The "no-gap" structure and thin carbon paper electrodes enables lower ohmic resistances in the cell due to better contact between components and lower charge transfer distances across the cell. In addition, the application of a serpentine flow channel greatly enhances the mass transfer in the porous electrode by distribution of the electrolyte across the entire membrane surface area. Nonetheless, additional performance enhancement of the VRB is considered possible through advanced architecture and material engineering. It is envisaged that performing similar pre-treatments to the carbon paper electrode as for CFs and GFs may improve the performance of the VRB significantly [73,74]. This is because carbon and graphite materials have a neutral wettability to water [142] which prevents the spreading of electrolyte over the electrode surface [5]. The trapped air pockets resulting from incomplete wetting reduce the electroactive surface area owing to the Cassie–Baxter effect. Other researchers also report similar results [143,144].

The application of carbon paper electrodes in hydrogen/bromine RFBs results in excellent performance (including a peak power density of 1.4 W cm^{-2}, a 91% voltaic efficiency at 0.4 W cm^{-2} constant-power operation and a fast responding system) [145]. Also cycling performance appears to be good but with some reversible decay.

3.11. Miscellaneous

Many carbon-based materials have been used as VRB electrode materials, such as CFs [43], carbon cloth [77], graphite powder [146], carbon black [69] and so on. These materials, however, have shown poor electrochemical activity towards the redox couples [43]. So it has been considered important to develop novel electrodes with high electrochemical activity. Graphite oxide (GO) is a graphite-based material which contains plenty of oxygen functional groups on basal planes and sheet edges [147–149] and shows exciting catalytic properties for the VRB redox couples [150]. The GO has been used as an electrode reaction catalyst when it is added into the graphite to obtain a novel graphite/GO composite electrode [46]. The composite electrode is suitable to be used as positive and negative electrodes in VRB electrolytes, which displays better performances with a higher peak current density and a lower charge transfer resistance of the electrode reactions in comparison with a single graphite electrode. The improvement of the electrochemical activity of the electrode can be associated to the existence of oxygen functional groups and extra specific surface areas induced by the GO. The enhanced electrochemical activity of the electrode is expected to increase the energy efficiency of VRBs in future studies.

The CV obtained at a GC electrode in a 1 M $VOSO_4$/2 M H_2SO_4 solution at different scan rates is displayed in Fig. 10 [151]. The anodic peak at about 1000–1100 mV corresponds to the oxidation of VO^{2+}–VO_2^+ [22]. The corresponding reduction peak occurs at about 700 mV during a negative scan. The anodic peak at about −400 mV and the cathodic peak at about −750 mV correspond to the oxidation and reduction of the redox couple of V^{2+}/V^{3+}, respectively. The large peak separation between anodic and cathodic peaks (>200 mV even at a low scan rate of 100 mV s^{-1}) suggests a slow kinetics for the electrochemical reactions of both the VO_2^+/VO^{2+} and V^{3+}/V^{2+} redox couples. Thus, electrodes are often optimised to maximise the electrochemical activity of redox electrolytes. One study also shows that the VO_2^+/VO^{2+} reaction changes from irreversible to reversible when the exchange current density increases by 2 orders of magnitude at a GF electrode [152,153]. The reduction of di-oxo-vanadium (5+) ion (VO_2^+) has fundamentally been investigated recently using glassy carbon rotating disk electrodes (GC RDEs) as a model of the carbon electrodes of VRBs [154]. The enrichment of oxygen-containing functional groups on the GC surface is performed by means of electrochemical oxidation. The enrichment enhances the VO_2^+ reduction and changes the Tafel slope from −0.161 to −0.087 V $decade^{-1}$, indicating the reduction mechanism alteration. The Tafel slope is explained by a multi-step reaction mechanism, in which the reduction of the quinone-like functional group generates the hydroxylic functional group that serves as the reaction site and coordinates to the oxo/di-oxo-vanadium (4+/5+) species.

A titanium plate with carbon films (TPCF) prepared by electrodeposition in a LiCl–KCl–K_2CO_3 melt was used as the electrode for VRBs [155]. The electrochemical behaviour of V^{2+}/V^{3+} and VO^{2+}/VO_2^+ redox couples on a TPCF electrode was investigated by CV, potentiodynamic polarisation and impedance techniques. The results showed that the V^{2+}/V^{3+} redox couple displayed a quasi-reversible process on the TPCF electrode, but, the VO^{2+}/VO_2^+ redox couple presented an irreversible process. The carbon atoms on surface of the TPCF electrode could be oxidised when the

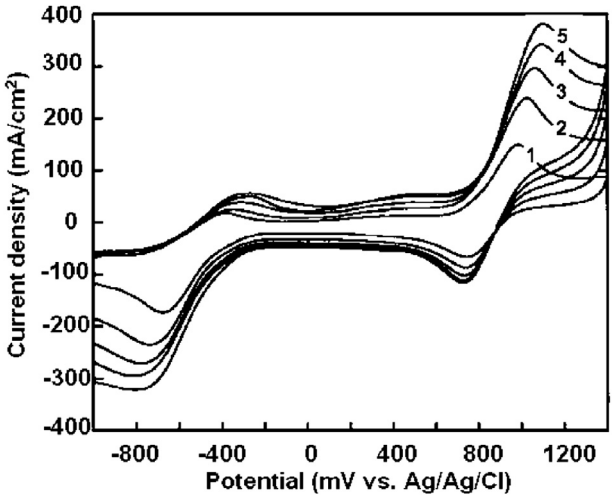

Fig. 10. CV obtained at a GC electrode in 1 M $VOSO_4$–2 M H_2SO_4 solution; scan rates: (1) 100, (2) 200, (3) 300, (4) 400, and (5) 500 mV s^{-1}. Reproduced from Yang et al. [22], copyright ACS as well as from Fang et al. [151], copyright Springer.

potential reached 1.5 V, which meant that the TPCF electrode had lower corrosion resistance than graphite electrodes.

Lopez-Atalaya and co-workers [156] investigated the behaviour of the Cr^{3+}/Cr^{2+} reaction on gold/graphite electrodes and concluded that the use of gold as a catalyst for Cr^{3+}/Cr^{2+} in an ICB was unnecessary for the acceptable behaviour of the RFB [22]. Carbon-based electrode materials were used in PSBs [15,55] and ZBBs [157] as well but no commercial success was ever reported [22].

Non-woven carbon base layer (gas diffusion layer) has been employed in VRBs to rebalance the cells. Whitehead and Harrer [158] have also used carbon paper electrodes loaded with 2.5 mg cm^{-2} of Pt–Ru catalyst as well for the same purpose. Their results show that the application of CF reduces the amount of catalyst loading and gives similar performance. Charge balance ensures better electrolyte utilisation.

4. Advances in nanotechnology and the application of GN in RFBs

More recently, CNTs, especially single walled CNTs (SWCNTs) have been intensively studied [159,160], but such materials are associated with disadvantages of very high cost, difficulties in preparation, problems in the reproducibility of surface structure/chemistry and limited purity. In contrast, graphene (GN) [161–165] has shown much promise due to its unique physical, chemical and thermal properties [166]. Among such properties, a high electrical conductivity, a high surface area, a widely applicable electrochemical activity and its relatively low production costs make GN an ideal material for application in greener and more energy-efficient storage/generation devices such as supercapacitors [167], lithium-ion batteries [168] or fuel cells [169]. Despite the increasing interest in GNs for electrochemical applications, the use of these materials as electrodes in RFBs has seen limited investigations [37,150].

The typical electrode materials used in VRBs showed poor kinetic reversibility towards the electrode reactions, so much attention was paid to their modification to improve the electrochemical activities [36,73,74]. In this regard, multi-walled CNTs (MWCNTs) and functional MWCNTs [170–175] were recently used as an electrode reaction catalyst by Li and co-workers [176] and their performances were investigated for the VO_2^+/VO^{2+} redox couple for VRBs. The electrochemical activities of the redox couple were greatly increased over those of modified GC electrodes and the electrocatalytic kinetics of the redox reactions were in the order of carboxyl MWCNTs > hydroxyl MWCNTs > pristine MWCNTs. The peak currents of the redox reactions (63.8 and −51.1 μA for oxidation and reduction processes, respectively) on the electrode modified by carboxyl MWCNTs were about three times higher than those for the other electrodes. The battery showed excellent storage efficiency when the carboxyl MWCNTs were used as positive electrode reaction catalysts, suggesting that the oxygen functional groups, especially the carboxyl, could significantly facilitate the VO_2^+/VO^{2+} redox reactions.

Recent studies have also shown that electrochemical activity of the FSWCNTs-modified electrodes (functionalised SWCNTs with large numbers of oxygen-containing groups) for the Br^-/Br_3^- redox couple reactions (for the V/Br RFB) is greatly increased relative to graphite and other CNT-modified electrodes and the electrochemical kinetics of the redox reactions are in the order of FSWCNTs > SWCNTs > MWCNTs > graphite [177]. This result suggests that the oxygen functional groups significantly facilitate the electron transfer processes, by providing active sites for the reactions and enhancing the effective carbon electrode area.

Other previous studies identified carbon fibres [42], nitrogen-doped mesoporous carbon (N-MPC) [36] and carbon black [69] as carbonaceous materials suitable for VRB electrodes. GN was considered a favourable electrode material because of its large surface area (2630 $m^2\ g^{-1}$) [178–181], which enhanced quantities of ionic adsorption and improved the electrochemical performance of any redox reaction.

Two GN-like materials suitable for use as positive electrodes in a VRB were obtained by thermal exfoliation and reduction of GO [37]. After thermal reduction, the electrocatalytic activity of thermally reduced and exfoliated graphene oxide (GNO) at 700 °C and 1000 °C, respectively (TRG700 and TRG1000) towards the redox reactions associated with VO_2^+/VO^{2+} was markedly enhanced with respect to the use of GNO only. In particular, TRG1000 showed a very good electrochemical performance in terms of peak current densities (30.54 and 30.05 mA cm^{-2} for the anodic and cathodic peaks at 1 mV s^{-1}, respectively) and reversibility, reaching a peak potential separation value (ΔE_p) of 0.07 mV. These excellent results were attributed to the restoration of carbon's sp^2 domains after thermal treatment, which implied the production of a GN-like material with a high electrical conductivity and accessible surface area [162]. Moreover, the residual functional groups, –OH, behaved as active sites towards the vanadium redox reactions. This represented a significant step forward in the development of highly effective VRB electrode materials.

Furthermore, Ir nanoparticles can be deposited onto GN to prevent it from restacking, thereby increasing its electrochemical performance [103,182]. A new study has been performed in the preparation of an Ir-decorated GN (Ir-GN) electrode by conducting synchronous reduction. GO and iridium chloride hydrate ($IrCl_3 \cdot 3H_2O$) have been utilised as precursors of GN and Ir, respectively, and Na borohydride ($NaBH_4$) is used as the reducing agent. The physicochemical properties are characterised using X-ray diffraction (XRD) and X-ray photoelectron spectroscopy (XPS). Transmission electron microscopy (TEM) and CV are employed to assess the morphology and electrochemical behaviour of all samples. The results have revealed that Ir-GN electrodes may substantially enhance the level of electrochemical activity, because of the presence of an Ir decoration and is a promising electrode for implementation in future VRB studies.

Tsai et al. [61] describe the preparation of GN-modified graphite (GMG) composite electrodes with various weight ratios of GN–graphite. The authors have found that the use of the GMG composite electrodes can provide substantial improvements in the level of electrochemical activity as a result of the presence of GN and may be superior to conventional PAN-based GF electrodes in VRBs [183]. The addition of 3 wt.% GN in particular, produces a well-dispersed morphology within the graphite matrix, which is observed using field emission SEM [61]. A 30% improvement in the peak current densities of both oxidation and reduction in comparison to those of pristine graphite are ascribed to the presence of GN with exceptional electrochemical properties and residual oxygen-containing functional groups. The findings of Tsai and co-workers indicate that the use of GMG composite materials may be beneficial for the fabrication of electrodes in VRBs [16,184].

Nitrogen-doped carbon nanostructured materials have been shown to exhibit higher electrocatalytic activity in many electrochemical devices such as fuel cells [185–190] and biosensors [191]. In a new study the electrochemical redox behaviour of the VO^{2+}/VO_2^+ couple on nitrogen-doped mesoporous carbon (N-MPC) electrode is shown to give much higher performance than the widely used graphite [36]. The MPC was prepared using a soft-template method and doped with nitrogen by heat-treating MPC in ammonia. The electrocatalytic kinetics of the redox couple VO^{2+}/VO_2^+ was significantly enhanced on N-MPC electrodes compared

with MPC and graphite electrodes on their own. The reversibility of the redox couple VO^{2+}/VO_2^+ was greatly improved on N-MPC (0.61 for N-MPC vs. 0.34 for graphite), which was expected to increase the energy storage efficiency of RFBs. Nitrogen doping improved the electron transfer on electrode/electrolyte interface for both oxidation and reduction processes. N-MPC was a promising material for RFBs. This result also opened up new and wider applications of nitrogen-doped carbon materials.

Wang and co-workers [89] have successfully grown N-CNTs on GF by a chemical vapour deposition method. The ideal porous GF substrate provides a superior porous framework for the growth of CNTs (un-doped and doped with nitrogen). The CNTs (or N-CNTs) on the surface of GF significantly improves the electrochemical surface area of the carbon materials due to their relatively small size (~30 nm in diameter and several μm in length), thus resulting in higher performance in VRBs as shown in Fig. 11 [89]. The enriched porous structures of CNTs or N-CNTs on GF facilitate the diffusion of electrolyte in the VRB system. In addition, the N-doping enhances the electrode and thus battery performance because of the modified electronic and surface properties of CNTs on GF. The enriched porous structure of N-CNTs on GF facilitates the diffusion of electrolyte, while the N-doping significantly contributes to the enhanced electrode performance. Specifically, the N-doping (i) modifies the electronic properties of CNTs and alters the chemisorption characteristics of the vanadium ions, (ii) generates defect sites that are electrochemically more active, (iii) increases the oxygen species on CNT surfaces, which is a key factor influencing the VRB performance and (iv) makes the N-CNT electrochemically more accessible than the CNT on its own.

A new method was proposed to modify CF electrodes in order to stabilise the carboxyl MWCNTs on the carbon fibres. This was also accompanied by a procedure to improve catalytic properties of Nafion so that it could serve as an agglomerant for attaching carboxyl MWCNTs onto the CF to form an integer composite electrode [47]. In this way, the stability of the MWCNTs on the carbon fibres in flowing electrolytes was guaranteed by Nafion. The composite electrode was tested in the VRB practically and displayed excellent electrochemical activity and durability. The VO_2^+/VO^{2+} and V^{3+}/V^{2+} redox couples showed the best reversibility on the modified CF with MWCNT content of 4.47 wt.%. The advanced activities were mainly attributed to the catalytic properties of the carboxyl groups towards the redox reaction and the high electrical conductivity of the MWCNTs [173]. In addition, the loading of the MWCNTs in flowing electrolyte remained stable due to the adhesive properties of Nafion. Other catalysts were also introduced onto the surface of carbon fibres in a similar manner. The improvement in the performance of CF modified electrodes in VRBs was expected to enhance its commercial potential [47].

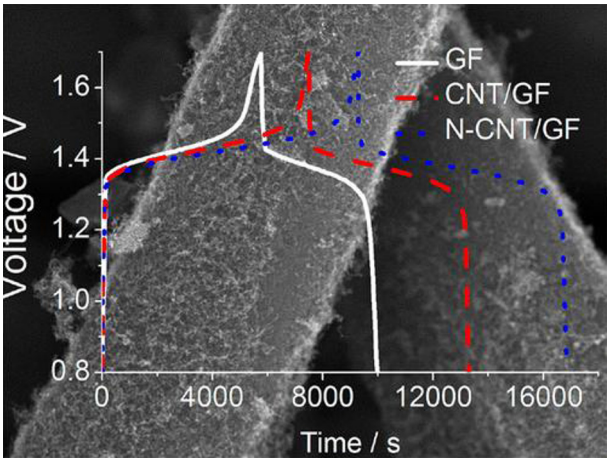

Fig. 11. SEM image and charge/discharge curves for CNT grown GFs employed in VRBs. Obtained from Wang et al. [89], with permission from ACS.

GNO nanoplatelets (GONPs) demonstrated a more favourable electrocatalytic activity for VO_2^+/VO^{2+} and V^{3+}/V^{2+} redox couples than pristine graphite for the VRB. It was found that the V^{3+}/V^{2+} redox reaction strongly depended on the formation of surface active functional groups of C–OH and COOH [5,150].

To take advantage of the superior electrical conductivity and mechanical properties of CNTs, several researchers [146,176] suggested a graphite–carbon nanotube composite for the VRB. Despite the significant advantages of CNTs, the sole use of CNTs in a vanadium reaction was found to give poor reversibility and activity compared to pure graphite [6]. In order to benefit from both graphite and CNTs, a composite of graphite with 5 wt.% CNTs was introduced that exhibited good reversibility and electrical conductivity. In another work, a GONP electrode was suggested for VRB by Han et al. [150]. This material did not require tedious synthesis procedures and had good catalytic property for both V^{2+}/V^{3+} and VO_2^+/VO^{2+} redox reactions due to the presence of C–OH and COOH functional groups on the electrode surface [6]. Polarisation of the GONP was further reduced after thermal treatment at a temperature of 120 °C. Furthermore, the authors prepared a GNO nanosheet/MWCNT hybrid electrode by an electrostatic spray technique and found that the electrode showed excellent electrocatalytic redox reversibility towards the VO_2^+/VO^{2+} couple, especially for the reduction from VO_2^+ to VO^{2+} [192].

Friedl and co-workers [193] presented a novel way to determine the charge transfer kinetics of redox reactions on porous MWCNT electrodes and detected a catalytic behaviour of surface functional groups towards the Fe^{2+}/Fe^{3+} reaction. This was, however, not the case for the VO^{2+}/VO_2^+ redox couple. Therefore it was concluded that polar molecules played no role in the redox reaction and a proposition was made that such molecules actually slow down the reaction by decreasing the mobility of the vanadium ions. The described method made it possible to compare the suitability of various electrode materials for their applicability in RFBs, without having to know the exact surface area, electrode geometry and porosity.

A recent study [194] has focused on the characteristics and performance of a novel electrode for the cathodic reaction of a VRB based on:

(i) Chemical activation of 2D GN electrode material using $CuPt_3$ nanocube bimetallic nanoparticles, chosen as a preliminary stoichiometric combination, morphology and size whose effect has been compared with that of Pt nanocubes [28].
(ii) Thermal activation under NH_3/O_2 (1:1) atmosphere in different temperatures and times applied to a 3D PAN-based graphite felt electrode. Large amounts of N- and O-containing groups have been introduced onto the surface electrode [167].

Both activations applied to carbon materials lead to modify the electron-donor properties of the surface enhancing the oxygen transport processes involved in the reaction for V(IV)/V(V) [66]; this causes a fast faradaic redox reaction (i.e., accelerates the oxygen and electron transfer processes in the electrode/electrolyte interface by the presence of oxygen-containing groups at the surface of the electrode) [194]. The modified electrodes show good morphological properties and large electrochemical surface area. Furthermore, the performance and longevity of the VRB single-cell prototype using dPAN (500, 24) electrode have been evaluated showing an energy efficiency of 84% (85% of voltage and 99% of

Table 3
Details of C and C-based electrodes employed in different RFBs. OCP stands for open circuit potential. Some parts may be similar to the authors' previous review [2] (with permission from ECS).

Ref.	Redox system	Electrode materials used	OCP (V)	Charge/discharge current density (mA cm^{-2})	Charge/discharge efficiency (%)
[55]	PSB	Activated C (AC)/polyolefin pressed electrodes or Ni foam/CF materials.	1.7–2.1	40	77.2
[57]	Soluble Pb/H_2SO_4	Positive and negative electrodes made of 70 ppi RVC and 40 ppi reticulated Ni were employed, respectively.	1.62	20	60–66 (overall)
[73,74]	VRB	GF electrodes heat bonded on C-filled polyethylene (PE) conducting plastic bipolar substrates were employed initially. Afterwards thermally and chemically treated GFs were used.	1.6	10–130	83
[130]	V-Polyhalide	Glassy carbon (GC) sheets were used as current collectors and GF was employed as the electrode material in both half cells.	1.3	20	66.4
[195–198]	ICB	Early studies used 1/8 in. C felt (CF) electrodes with traces of Pb (100–200 μg cm^{-2}) and gold (Au) (12.5 μg cm^{-2}) deposited on the Cr electrode. Later on, reticulated vitreous C (RVC) pre-treated with methanol was employed. Much later work ensured the use of thermally treated graphite felt (GF).	1.18	21.5	95 (coulombic)
[199–202]	Iron/Titanium (Fe/Ti)	G foil electrodes were compared with platinised platinum (Pt) foil and a Ti-based chlorine anode. G foil gave better efficiencies.	1.19	14	44–50 (overall)
[135]	$[Ru(bpy)_3](BF_4)_2$[a]	C fibre cloth electrodes were employed in a flow-by configuration. For more information on flow-through or flow-by porous electrode assemblies, the reader is referred to publications by Langlois and Coeuret [203].	2.6	3 V to 50% SOC (charge) 5 (discharge)	18 (overall)
[204]	V/Br	CF or GF bonded onto conductive plastic sheets were employed.	1.4	20	74
[205]	Magnesium/V	Polyacrylonitrile (PAN) based CF or spectral pure G electrodes were employed.	1.66	20	63
[206]	Zn/Ce	C plastic anodes and platinised Ti mesh cathodes of 100 cm^2 geometrical area.	2.45	50	98 (coulombic)
[206,207]	V/Ce	C fibres of 10 μm diameter as negative electrodes were filled inside a cylindrical membrane. 4 bundles of the C fibres were arranged evenly around the outside of the membrane to act as positive electrodes.	1.5	22	90 (coulombic)
[208]	V-glyoxal (O_2)	G plates and porous GFs were used as current collectors and electrodes, respectively.	1.2	20	66 (coulombic)
[209]	V-cystine (O_2)	2.5 mm thick GFs (dimension: 25 mm × 20 mm) were contacted against G plates that served as current collectors.	1.3	20	58 (overall)
[210]	V acetylacetonate	GF electrodes	2.2	2.2 (charge) 0.2 (discharge)	47 (coulombic)
[211]	ZBB	Two C electrodes of 60 cm^2 with a 5 mm inter-electrode gap were employed.	1.6	15	80
[212,213]	All-Neptunium	c-Plane C of pyrolytic G and plastic formed C.	1.3	70	99.1 (predicted via mathematical modelling)
[214,215]	All-Cr (aqueous)	GF electrodes were thermally pre-treated at 500 °C in a muffle furnace to reduce its hydrophobic nature.	2.11	30 (during charge) 2.5 (during discharge)	15% with stationary H-type cell 7% with undivided RFB
[216]	All-Cr (organic) – used in H-type cell	GF electrodes	3.4	0.14 (charge) 0.014 (discharge)	20
[217]	Manganese acetylacetonate	GF electrodes	1.1	0.14 (charge) 0.014 (discharge)	21
[218]	Tiron[a]	A GF (10 mm thick) contacted against one G plate was used as the working electrode. Pb and a saturated calomel electrode (SCE) were used as the counter and reference electrodes, respectively.	1.1	10	82
[219,220]	Ruthenium (Ru) acetylacetonate	GF electrodes in undivided flow-through electrochemical reactor	1.76	0.28 (charge) 0.056 (discharge)	5
[221]	$Ni(bpy)_3/Fe(bpy)_3$[a]	GF electrodes	2.25	0.8	88.1
[222]	TEMPO[a]/*N*-methylphthalimide	GF electrodes	1.6	0.35	90
[223–225]	$CuCl_2$ dissolved in deep eutectic solvent (ethaline[a])	C cloth	0.77	7.5	62
[226]	Semisolid lithium flow cell (SSFC)	Anode is a lithium foil material while the cathode is a G plate	4.7	2 and 4.4 V	22
[227]	Iron-ion/Hydrogen redox flow cell	Platinum/Carbon anode and CF cathode with G current collector blocks	0.75	25	40–80

[a] $[Ru(bpy)_3](BF_4)_2$ = tris(2,2′-bipyridine) Ru (II) tetrafluoroborate; Tiron = 4,5-dihydroxy-1,3-benzenedisulfonic acid, disodium salt monohydrate; $Ni(bpy)_3/Fe(bpy)_3$ = Ni and Fe tris(2,2′-bipyridine); TEMPO = 2,2,6,6-tetramethyl-1-piperidinyloxy; Ethaline = deep eutectic solvent formed from the hydrogen bond of choline chloride and ethylene glycol.

current efficiencies respectively) at a current density of 20 mA cm^{-2} up to 30 cycles, leading to a step forward towards scaling-up the VRB.

5. Conclusions

Carbon-based electrodes have been applied in RFBs since the 1970s. A range of different carbon- and graphite-based architectures has been studied over the years and the performance of such electrodes in RFBs have been summarised in Table 3 (in terms of energy efficiencies only). Varying reports are given in the literature regarding RFB energy efficiencies and power densities. However, it is clear from Tables 2 and 3 that mainly carbon paper and graphite felt electrodes result in optimum performance in terms of high redox rate constants and energy efficiencies, respectively.

In addition, it is reported that several surface treatments can lead to improved reaction kinetics on carbon electrodes. Chemical etching, thermal treatment, chemical doping, CNT or GN addition and application of metallic catalyst sites to carbon fibres have all been studied in depth. Besides catalytic activity, the carbon- and graphite-based electrode materials have good electrical conductivity, chemical stability and robustness in the reaction environment. This explains their widespread application in the RFB till date (the main variants studied are CF, GF, PAN-based GF, GF bonded with conducting plastic, AC, RVC, carbon paper, carbon or graphite cloth and a range of other miscellaneous assemblies such as CNTs or GN-modified carbon electrodes).

6. Challenges and opportunities

Overall, the combination of the right electrode materials with a proper electrolyte can successfully increase both the energy stored by the device and its power, but no perfect active material exists and no electrolyte suits every material and every performance goal [228]. However, today, many materials are available, including porous activated, carbide-derived, and templated carbons with high surface areas and porosities that range from the sub-nm scale to just a few nm. If the pore size is matched with the electrolyte ion size, those materials can provide high energy density. Exohedral nanoparticles, such as carbon nanotubes and onion-like carbon, can provide high power due to fast ion sorption/desorption on their outer surfaces. Due to its higher charge–discharge rates compared with activated carbons, graphene has attracted increasing attention, but graphene has not yet shown a higher volumetric capacitance than porous carbons [229].

Although aqueous electrolytes, such as sodium sulphate, are the safest and least expensive, they have a limited potential window [228]. Organic electrolytes, such as solutions of tetraethyl ammonium tetrafluoroborate in acetonitrile or propylene carbonate, are the most common amongst non-aqueous devices [219,220,230]. Researchers are increasingly interested in non-flammable ionic liquids. These liquids have low vapour pressures, which allow them to be used safely over a temperature range from −50 to at least 100 °C and over a larger voltage window, which results in a higher energy density than other electrolytes. However, most of the work reported on ionic liquids in combination with carbon-based electrodes has been limited to areas outside the scope of RFBs to date. The main reports on RFBs, in this regard, have been from Sandia National Laboratories [231,232], Tianjin University [233] Aalto University [224] and the University of Malaya [223,225,234,235].

In order for RFB to find a place commercially, it is paramount that the costs and benefits associated with both purchasing and maintaining a system are as attractive as possible. Recent research by Moore et al. [236] in this regard has shown that many of the key costs associated with RFB systems are directly related to the initial procurement costs of materials used to construct the system, including electrodes. Therefore, without developing new materials for RFB systems, the next most cost-effective method of reducing initial expenditure is to improve overall cell performance. It is here that carbon-based electrodes can play a significant role. Consequently, an improvement in cell performance would deliver a reduction in stack size and its associated costs while meeting the same power requirements [140,237–240].

In this regard, an unexplored area with immediate application would be to understand how three sources behind overpotential losses (i.e., ion convection, counter-ion counter-diffusion and boundary layer diffusion) can be overcome. Ideally, higher levels of charge flux for pumping anion/cations between carbon-based electrodes would help mitigate these effects but is currently not understood [9]. Furthermore, the dependence of the VO_2^+/VO^{2+} couple on the carbon electrode material has also not been well studied [5]. Additionally, the production of carbon-based electrodes with much lower contact resistances than conventional electrodes [136] may be possible through harnessing of ionic liquid functionalisation of GNs and CNTs, produced through exfoliation of graphite [161,241,242]. This would result in improving RFB efficiencies and power densities.

The aptitude to predict cell degradation is a challenge because for different RFB systems the mechanisms are usually diverse [6,243]. For instance, Thompson and co-workers [243] have found that environmental oxygen and water tends to result in side reactions that affect the performance of non-aqueous VRBs adversely. Additional experimental data on the degradation mechanisms of other RFB systems (especially work that focus on carbon-based electrodes), however, are not reported so extensively as for the non-aqueous VRB, due to which, quantitative cause-and-effect relationships between observation and degradation pathways are arduous to acquire.

During a lifetime of operation, carbon-based electrodes may suffer from mechanical, thermal, or electrochemical sources of degradation. Mechanical separation would result in the loss of active surfaces, block pores and may increase stresses in other parts of the carbon electrode. Thermal differences would affect mechanical and thermal expansion of carbon, chemical reaction rates and concentration profiles. Electrochemically depending on load, differences in localised current densities within the carbon microstructure could affect concentration profiles, may induce heating and couple with mechanical/thermal processes at work. The dominant mechanism behind degradation for each case in turn will depend on the operating conditions of the RFB. The presence of localised inhomogeneities (e.g. current densities) driven through microstructural differences within the electrode may also accentuate failure in particular regions of the electrode given sufficient time. As is evident, decoupling and understanding the cause behind observed degradation effects is therefore difficult.

Recent progress in three-dimensional (3D) imaging/tomography techniques can provide insight into the nano/micro structure of electrodes that can help deconvolute some of these effects [244]. Once the actual 3D microstructure is captured it is possible to understand spatial relationships of particles/phases/fibres/thicknesses with each other and how these change in a quantitative manner under a controlled set of conditions. Furthermore structures captured in this manner offer the potential to be cycled and re-analysed (so called 4D time resolved data) or used as real geometric input for models to correlate with observed behaviour [244–247].

Unfortunately, experimental procedures for determining 3D microstructural information have been reported in-depth for lithium batteries or fuel cells [244–252]. Two familiar techniques

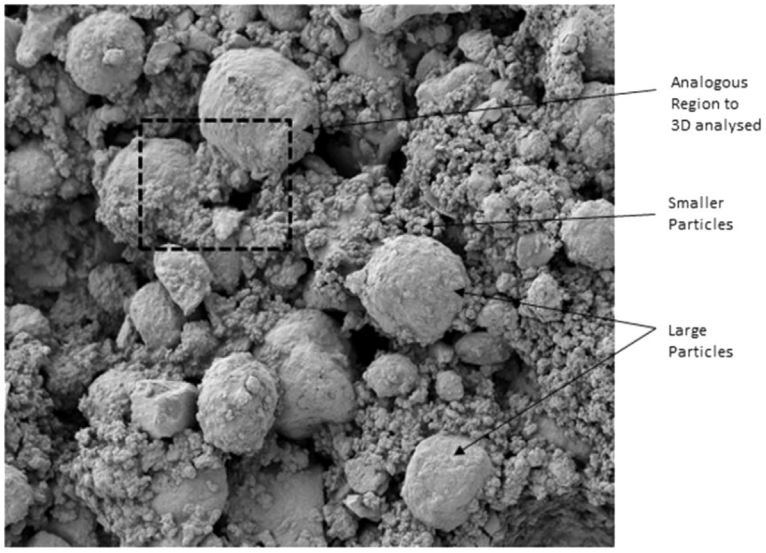

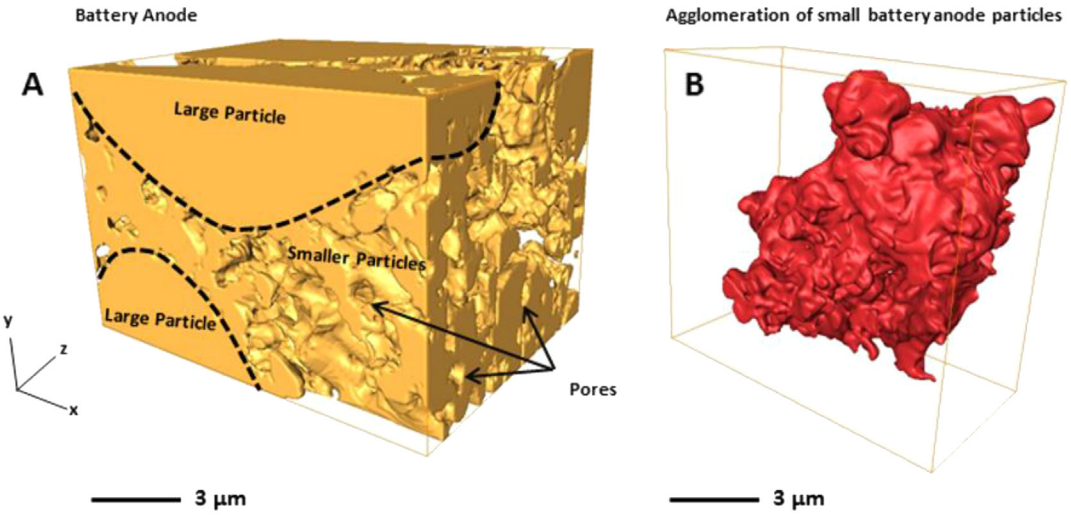

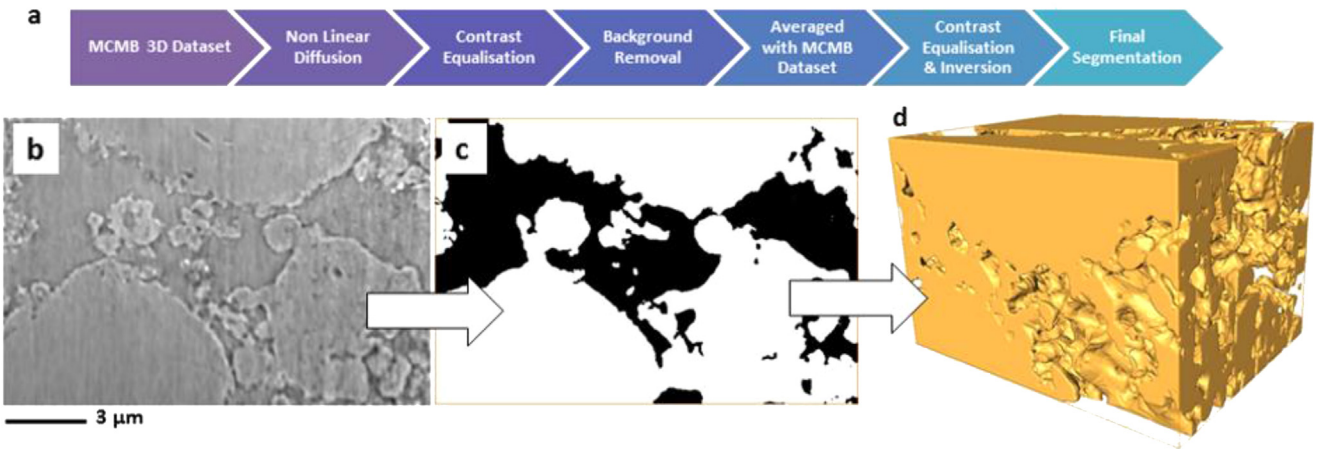

Fig. 12. (a) Graphite anode microstructure (A: 3D MCMB or mesocarbon microbead based battery anode microstructure using 3D tomography; B: Microstructure of an agglomeration of smaller particles segmented from the bulk reconstruction); (b) original reconstructed slice from X-ray nano computed tomography; (c) segmented MCMB structure following feature extraction; (d) rendering of the 3D battery anode microstructure following segmentation [260] (with permission from Elsevier).

employed in most cases involve high resolution X-ray computerised tomography and focused ion beam tomography [253–259].

Collectively, therefore the 3D imaging work on carbon-based materials has shown an ability to quantify surface areas, volumes, particle sizes, porosity, identify different phases, determine tortuosity and flow characteristics of complex structures [260–262]. All of the structures captured can also be used as geometric inputs to model cell behaviour (as illustrated in Fig. 12). It is therefore remarkable, that, to date there have been little 3D reconstructions of a carbon-based RFB electrode presented in the literature.

Some of the works reported so farutilise X-ray tomography to model the effect of concentration, overpotential and charge density within a RFB [263]. This has been developed further by Qui et al. [264] who have demonstrated the effects of real pore/electrode morphology acquired using X-ray tomography on electrochemical performance. They have reported cell voltage to rise with increasing electrolyte flow rate as a result of decreasing concentration gradients. Their simulations suggest a detrimental effect on RFB performance in the event of fuel starvation/low flow rates/low electrolytic concentrations. Therefore while little work in this area has been carried out to date, it is likely to provide insights important for cell performance that are currently not known and presents a gap in the body of literature.

Further work is necessary in this regard to quantify and thereby understand the effects of micro/nano structure on RFB degradation mechanisms. This enables better battery electrodes to be developed that can improve cell performance so that such progress may help the technology reach commercial success.

Acknowledgements

The authors are grateful to the University of Malaya and the Ministry of Higher Education in Malaysia for supporting this collaborative work by means of the research grant UM.C/HIR/MOHE/ENG/18 which made it possible for an extended visit of MHC to Imperial College London. MHC is also grateful to the European Commission Seventh Framework Programme (Capacities) for partly funding this work via the BRISK programme (PAB P91059).

References

[1] M.H. Chakrabarti, S.A. Hajimolana, F.S. Mjalli, M. Saleem, I. Mustafa, Arab. J. Sci. Eng. 38 (2013) 723–739.
[2] M. Skyllas-Kazacos, M.H. Chakrabarti, S.A. Hajimolana, F.S. Mjalli, M. Saleem, J. Electrochem. Soc. 158 (2011) R55–R79.
[3] T. Shigematsu, SEI Tech. Rev. 73 (2011) 4–13.
[4] P. Alotto, M. Guarnieri, F. Moro, Renew. Sustain. Energy Rev. 29 (2014) 325–335.
[5] A.Z. Weber, M.M. Mench, J.P. Meyers, P.N. Ross, J.T. Gostick, Q. Liu, J. Appl. Electrochem. 41 (2011) 1137–1164.
[6] P. Leung, X. Li, C. Ponce de León, L. Berlouis, C.T.J. Low, F.C. Walsh, RSC Adv. 2 (2012) 10125–10156.
[7] S.-H. Shin, S.-H. Yun, S.-H. Moon, RSC Adv. 3 (2013) 9095–9116.
[8] H. Prifti, A. Parasuraman, S. Winardi, T.M. Lim, M. Skyllas-Kazacos, Membranes 2 (2012) 275–306.
[9] D. You, H. Zhang, J. Chen, Electrochim. Acta 54 (2009) 6827–6836.
[10] G.J. Suppes, B.D. Sawyer, M.J. Gordon, AIChE J. 57 (2011) 1961–1967.
[11] P.K. Leung, C. Ponce-de-Leon, C.T.J. Low, A.A. Shah, F.C. Walsh, J. Power Sourc. 196 (2011) 5174–5185.
[12] G. Nikiforidis, L. Berlouis, D. Hall, D. Hodgson, J. Power Sourc. 206 (2011) 497–503.
[13] M. Skyllas-Kazacos, F. Grossmith, J. Electrochem. Soc. 134 (1987) 2950–2953.
[14] Y.J. Kim, H.J. Lee, S.W. Lee, B.W. Cho, C.R. Park, Carbon 43 (2005) 163–169.
[15] H.T. Zhou, H.M. Zhang, P. Zhao, B.L. Yi, Electrochim. Acta 51 (2006) 6304–6312.
[16] D. Pletcher, R. Wills, Phys. Chem. Chem. Phys. 6 (2004) 1779–1785.
[17] C.M. Hagg, M. Skyllas-Kazacos, J. Appl. Electrochem. 32 (2002) 1063–1069.
[18] D.S. Aaron, Q. Liu, Z. Tang, G.M. Grim, A.B. Papandrew, A. Turhan, T.A. Zawodzinski, M.M. Mench, J. Power Sourc. 206 (2012) 450–453.
[19] J. Jorné, J.T. Kim, D. Kralik, J. Appl. Electrochem. 9 (1979) 573–579.
[20] K. Kinoshita, S.C. Leach, J. Electrochem. Soc. 129 (1982) 1993–1997.
[21] Y.M. Zhang, Q.M. Huang, W.S. Li, H.Y. Peng, S.J. Hu, J. Inorg. Mater. 22 (2007) 1051–1056.
[22] Z.G. Yang, J.L. Zhang, M.C.W. Kintner-Meyer, X.C. Lu, D.W. Choi, J.P. Lemmon, J. Liu, Chem. Rev. 111 (2011) 3577–3613.
[23] M.Q. Zhang, M. Moore, J.S. Watson, T.A. Zawodzinski, R.M. Counce, J. Electrochem. Soc. 159 (2012) A1183–A1188.
[24] M.J. Watt-Smith, H. Al-Fetlawi, P. Ridley, R.G.A. Wills, A.A. Shah, F.C. Walsh, J. Chem. Technol. Biotechnol. 88 (2013) 126–138.
[25] Q. Liu, A. Turhan, T.A. Zawodzinski, M.M. Mench, Chem. Commun. 49 (2013) 6292–6294.
[26] Y.-K. Fuh, T.-C. Chang, J.-P. Zhang, Int. J. Electrochem. Sci. 8 (2013) 8989–8999.
[27] F. Mishra, F. Yang, R. Pitchumani, J. Fuel Cell Sci. Technol. 1 (2004) 2–9.
[28] J.G. Pharoah, J. Power Sourc. 144 (2005) 77–82.
[29] A. Tang, J. McCann, J. Bao, M. Skyllas-Kazacos, J. Power Sourc. 242 (2013) 349–356.
[30] C. Ding, H. Zhang, X. Li, T. Liu, F. Xing, J. Phys. Chem. Lett. 4 (2013) 1281–1294.
[31] L.H. Thaller, Electrically Rechargeable Redox Flow Cells, NASA TM X-71540, National Aeronautics and Space Administration, Washington, DC, 1974.
[32] L.H. Thaller, Inventor: electrically rechargeable redox flow cell. US Patent 3,996,064, 1976.
[33] L.H. Thaller, Inventor: electrochemical cell for rebalancing redox flow system. US Patent 4,159,366, 1979.
[34] A. Parasuraman, T.M. Lim, C. Menictas, M. Skyllas-Kazacos, Electrochim. Acta 101 (2013) 27–40.
[35] C. Ponce-de-Leon, G.W. Reade, I. Whyte, S.E. Male, F.C. Walsh, Electrochim. Acta 52 (2007) 5815–5823.
[36] Y. Shao, X. Wang, M. Engelhard, C. Wang, S. Dai, J. Liu, Z. Yang, Y. Lin, J. Power Sourc. 195 (2010) 4375–4379.
[37] Z. González, C. Botas, P. Álvarez, S. Roldán, C. Blanco, R. Santamaría, M. Granda, R. Menéndez, Carbon 50 (2012) 828–834.
[38] E. Sum, M. Rychcik, M. Skyllas-Kazacos, J. Power Sourc. 16 (1985) 85–95.
[39] E. Sum, M. Skyllas-Kazacos, J. Power Sourc. 15 (1985) 179–190.
[40] M. Inoue, Y. Tsuzuki, Y. Iizuka, M. Shimada, J. Electrochem. Soc. 134 (1987) 756–757.
[41] M. Skyllas-Kazacos, D. Kasherman, D.R. Hong, M. Kazacos, J. Power Sourc. 35 (1991) 399–404.
[42] L. Yue, W. Li, F. Sun, L. Zhao, L. Xing, Carbon 48 (2010) 3079–3090.
[43] W.H. Wang, X.D. Wang, Electrochim. Acta 52 (2007) 6755–6762.
[44] C.H. Chang, T.S. Yuen, Y. Nagao, H. Yugami, J. Power Sourc. 195 (2010) 5938–5941.
[45] C.T. Hsieh, H. Teng, W.Y. Chen, Y.S. Cheng, Carbon 48 (2010) 4219–4229.
[46] W. Li, J. Liu, C. Yan, Electrochim. Acta 56 (2011) 5290–5294.
[47] G. Wei, C. Jia, J. Liu, C. Yan, J. Power Sourc. 220 (2012) 185–192.
[48] F.C. Walsh, A First Course in Electrochemical Engineering, The Electrochemical Consultancy, Romsey, 1993.
[49] D. Pletcher, F.C. Walsh, Industrial Electrochemistry, second ed., Chapman-Hall, London, 1992.
[50] M. Kazacos, M. Skyllas-Kazacos, J. Electrochem. Soc. 136 (1989) 2759–2760.
[51] S. Zhong, M. Kazacos, R.P. Burford, M. Skyllas-Kazacos, J. Power Sourc. 36 (1991) 29–43.
[52] M.S. Yazici, D. Krassowski, J. Prakash, J. Power Sourc. 141 (2005) 171–176.
[53] P. Qian, H.M. Zhang, J. Chen, Y.H. Wen, Q.T. Luo, Z. Liu, D. You, B. Yi, J. Power Sourc. 175 (2008) 613–620.
[54] C. Herscovici, Inventor: porous and porous-nonporous composites for battery electrodes. US Patent 4,920,017, 1990.
[55] P. Zhao, H.M. Zhang, H.T. Zhou, B.L. Yi, Electrochim. Acta 51 (2005) 1091–1098.
[56] P.K. Leung, C. Ponce-de-León, C.T.J. Low, F.C. Walsh, Electrochim. Acta 56 (2011) 6536–6546.
[57] J. Collins, X. Li, D. Pletcher, R. Tangirala, D. Stratton-Campbell, F.C. Walsh, C. Zhang, J. Power Sourc. 195 (2010) 2975–2978.
[58] X.-G. Li, K.-L. Huang, S.-Q. Liu, N. Tan, L.-Q. Chen, Trans. Nonferrous Met. Soc. China 17 (2007) 195–199.
[59] X. Tang, J. Li, J. Hao, Catal. Commun. 11 (2010) 871–875.
[60] K.J. Kim, Y.-J. Kim, J.-H. Kim, M.-S. Park, Mater. Chem. Phys. 131 (2011) 547–553.
[61] H.-M. Tsai, S.-Y. Yang, C.-C.M. Ma, X. Xie, Electroanalysis 23 (2011) 2139–2143.
[62] P. Lessner, F. Mclarnon, J. Winnick, E. Cairns, J. Appl. Electrochem. 22 (1992) 927–934.
[63] W. Lu, D.D.L. Chung, Carbon 40 (2002) 447–449.
[64] V. Haddadi-Asl, M. Kazacos, M. Skyllas-Kazacos, J. Appl. Electrochem. 25 (1995) 29–33.
[65] V. Haddadi-Asl, M. Kazacos, M. Skyllas-Kazacos, J. Appl. Polym. Sci. 57 (1995) 1455–1463.
[66] D.A. Szánto, Characterization of Electrochemical Filter-Press Reactor, PhD Thesis, University of Portsmouth, UK, 1999.
[67] E.H. Weber, Development and Modeling of Thermally Conductive Polymer/Carbon Composites, PhD Thesis, Michigan Technological University, USA, 2001.
[68] K. Robberg, V. Trapp, Graphite-based bipolar plates. Handbook of Fuel Cells, John Wiley & Sons, New York, 2010.
[69] G.J.W. Radford, J. Cox, R.G.A. Wills, F.C. Walsh, J. Power Sourc. 185 (2008) 1499–1504.

[70] A. Brungs, V. Haddadi-Asl, M. Skyllas-Kazacos, J. Appl. Electrochem. 26 (1996) 1117–1123.
[71] S. Zhong, M. Kazacos, Inventors: flexible, conducting plastic electrode and process for its preparation. US Patent 5,665,212, 1997.
[72] R. Carta, S. Palmas, A.M. Polcaro, G. Tola, J. Appl. Electrochem. 21 (1991) 793–798.
[73] B.T. Sun, M. Skyllas-Kazacos, Electrochim. Acta 37 (1992) 1253–1269.
[74] B.T. Sun, M. Skyllas-Kazacos, Electrochim. Acta 37 (1992) 2459–2465.
[75] M. Rychcik, M. Skyllas-Kazacos, J. Power Sourc. 22 (1988) 59–67.
[76] M. Rychcik, M. Skyllas-Kazacos, J. Power Sourc. 19 (1987) 45–54.
[77] H. Kaneko, K. Nozaki, A. Negishi, Y. Wada, T. Aoki, M. Kamimoto, Electrochim. Acta 36 (1991) 1191–1196.
[78] A. Paulenova, S.E. Creager, J.D. Navratil, Y. Wei, J. Power Sourc. 109 (2002) 431–438.
[79] H.J. Liu, Q. Xu, C.W. Yan, Y.L. Qiao, Electrochim. Acta 56 (2011) 8783–8790.
[80] B.T. Sun, M. Skyllas-Kazacos, Electrochim. Acta 36 (1991) 513–517.
[81] C. Fabjan, J. Garche, B. Harrer, L. Jörissen, C. Kolbeck, F. Philippi, G. Tomazic, F. Wagner, Electrochim. Acta 47 (2001) 825–831.
[82] Z. González, A. Sánchez, C. Blanco, M. Granda, R. Menéndez, R. Santamaría, Electrochem. Commun. 13 (2011) 1379–1382.
[83] K.J. Kim, M.S. Park, J.H. Kim, U. Hwang, N.J. Lee, G.J. Jeong, Y.-J. Kim, Chem. Commun. 48 (2012) 5455–5457.
[84] X. Li, K. Horita, Carbon 38 (2000) 133–138.
[85] C. Flox, J. Rubio-García, M. Skoumal, T. Andreu, J.R. Morante, Carbon 60 (2013) 280–288.
[86] L. Wang, J. Zhao, X. He, J. Ren, H. Zhao, J. Gao, J. Li, C. Wan, C. Jiang, Int. J. Electrochem. Sci. 7 (2012) 554–560.
[87] F. Lamouroux, S. Bertrand, R. Pailler, R. Naslain, M. Cataldi, Compos. Sci. Technol. 59 (1999) 1073–1085.
[88] T. Wu, K.L. Huang, S.Q. Liu, S.X. Zhuang, D. Fang, S. Li, D. Lu, A. Su, J. Solid State Electrochem. 16 (2012) 579–585.
[89] S. Wang, X. Zhao, T. Cochell, A. Manthiram, J. Phys. Chem. Lett. 3 (2012) 2164–2167.
[90] A. Stein, Z. Wang, M.A. Fierke, Adv. Mater. 21 (2009) 265–293.
[91] M.H. Chakrabarti, E.P.L. Roberts, J. Chem. Soc. Pak. 30 (2008) 817–823.
[92] M.H. Chakrabarti, E.P.L. Roberts, NED Univ. J. Res. 5 (2008) 43–59.
[93] M.H. Chakrabarti, R.A.W. Dryfe, E.P.L. Roberts, J. Chem. Soc. Pak. 29 (2007) 294–300.
[94] C. Bae, H. Chakrabarti, E. Roberts, J. Appl. Electrochem. 38 (2008) 637–644.
[95] X.G. Li, K.L. Huang, S.Q. Liu, L.Q. Chen, J. Cent. South Univ. Technol. 14 (2007) 51–56.
[96] N. Tan, K. Huang, S.-Q. Liu, X.-G. Li, Z.-F. Chang, Acta Chim. Sin. 64 (2006) 584–588.
[97] J. Xi, W. Zhang, Z. Li, H. Zhou, L. Liu, Z. Wu, X. Qiu, Int. J. Electrochem. Sci. 8 (2013) 4700–4711.
[98] E. Bulska, W. Jedral, E. Kopysc, H.M. Ortner, S. Flege, Spectrochim. Acta B Atom. Spectros. 57 (2002) 2017–2029.
[99] S.B. Hocevar, I. Svancara, K. Vytras, B. Ogorevc, Electrochim. Acta 51 (2005) 706–710.
[100] G.H. Hwang, W.K. Han, J.S. Park, S.G. Kang, Sensors Actuators B Chem. 135 (2008) 309–316.
[101] F. Arduini, J.Q. Calvo, A. Amine, G. Palleschi, D. Moscone, Trends Anal. Chem. 29 (2010) 1295–1304.
[102] H. Yang, C.-H. Hung, S.-P. Wang, I.-L. Chiang, Rare Met. 30 (2011) 1–4.
[103] H.-M. Tsai, S.-J. Yang, C.-C.M. Ma, X. Xie, Electrochim. Acta 77 (2012) 232–236.
[104] N. Kausar, R. Howe, M. Skyllas-Kazacos, J. Appl. Electrochem. 31 (2001) 1327–1332.
[105] Y.L. Yao, Y. Ding, L.S. Ye, X.H. Xia, Carbon 44 (2006) 61–66.
[106] S.Y. Qian, B.E. Conway, G. Jerkiewicz, Phys. Chem. Chem. Phys. 1 (1999) 2805–2813.
[107] A. Afkhami, B.E. Conway, J. Colloid Interface Sci. 251 (2002) 248–255.
[108] J. Niu, B.E. Conway, J. Electroanal. Chem. 546 (2003) 59–72.
[109] W.T. Mook, M.K. Aroua, M.H. Chakrabarti, C.T.J. Low, P.V. Aravind, N.P. Brandon, Electrochim. Acta 94 (2013) 327–335.
[110] F. Julien, M. Baudu, M. Mazet, Water Res. 32 (1998) 3414–3424.
[111] Z. Li, M. Kruk, M. Jaroniec, S.K. Ryu, J. Colloid Interface Sci. 204 (1998) 151–156.
[112] F.C. Walsh, Pure Appl. Chem. 73 (2001) 1819–1837.
[113] B.D. Sawyer, G.J. Suppes, M.J. Gordon, M.G. Heidlage, J. Appl. Electrochem. 41 (2011) 543–550.
[114] J.W. Burress, P. Pfeifer, P. Shah, G.J. Suppes, Inventors: high surface area carbon and process for its production. World Patent 2008058231, 2008.
[115] M. Gordon, G. Suppes, AIChE J. 59 (2013) 2833–2842.
[116] J. González-Garcia, P. Bonete, E. Exposito, V. Montiel, A. Aldaz, R. Torregrosa-Macia, J. Mater. Chem. 9 (1999) 419–426.
[117] J.M. Friedrich, C. Ponce-de-Leon, G.W. Reade, F.C. Walsh, J. Electroanal. Chem. 561 (2004) 203–217.
[118] M. Mastragostino, S. Valcher, Electrochim. Acta 28 (1983) 501–505.
[119] J.P. Schrodt, W.T. Otting, J.O. Schoegler, D.N. Craig, Trans. Electrochem. Soc. 90 (1946) 405–417.
[120] J.C. White, W.H. Powers, R.L. McMutric, R.T. Pierce, Trans. Electrochem. Soc. 91 (1947) 73–94.
[121] G.D. McDonald, E.Y. Weissman, T.S. Roemer, J. Electrochem. Soc. 119 (1972) 660–663.
[122] F. Beck, Inventor: lead batteries. US Patent 4,001,037, 1977.
[123] R. Wurmb, F. Beck, K. Boehlke, Inventors: secondary battery. US Patent 4,092,463, 1978.
[124] P.O. Henk, Z.A.A. Piontkowski, Inventors: lead salt electric storage battery. US Patent 4,331,744, 1982.
[125] P.O. Henk, Inventor: lead salt electric storage battery. US Patent 4,400,449, 1983.
[126] A. Hazza, D. Pletcher, R. Wills, J. Power Sourc. 149 (2005) 103–111.
[127] A. Hazza, D. Pletcher, Phys. Chem. Chem. Phys. 6 (2004) 1773–1778.
[128] D. Pletcher, R. Wills, J. Power Sourc. 149 (2005) 96–102.
[129] A. Shibata, K. Sato, Power Eng. J. 13 (1999) 130–135.
[130] M. Skyllas-Kazacos, J. Power Sourc. 124 (2003) 299–302.
[131] M. Skyllas-Kazacos, A. Mousa, M. Kazakos, Inventors: metal bromide redox flow cell, PCT Application, PCT/GB2003/001757, 2003.
[132] R.L. Clarke, B.J. Dougherty, S. Harrison, J.P. Millington, Inventors: battery with bifunctional electrolyte. US Patent Application, International publication WO 2004/095602 A2, 2004.
[133] L. Joerissen, J. Garche, C. Fabjan, G. Tomazic, J. Power Sourc. 127 (2004) 98–104.
[134] K. Huang, Q. Wu, S. Liu, J. Chin. Power Sourc. 2 (2004) 91–93.
[135] Y. Matsuda, K. Tanaka, M. Okada, Y. Takasu, M. Morita, T. Matsumura-Inoue, J. Appl. Electrochem. 18 (1988) 909–914.
[136] W.A. Braff, M.Z. Bazant, C.R. Buie, Nat. Commun. 4 (2013) 1–6.
[137] A.-Q. Su, N.-F. Wang, S.-Q. Liu, T. Wu, S. Peng, Acta Phys. Chim. Sin. 28 (2012) 1387–1392.
[138] M. Skyllas-Kazacos, C. Menictas, The vanadium redox battery for emergency back-up applications, in: Extended abstracts, 19th International INTELEC Telecommunications Energy Conference, IEEE, Victoria (Melbourne, Australia), 1997, pp. 463–471.
[139] D. Chen, S. Wang, M. Xiao, Y. Meng, J. Power Sourc. 195 (2010) 2089–2095.
[140] E. Kjeang, R. Michel, D.A. Harrington, N. Djilali, D. Sinton, J. Am. Chem. Soc. 130 (2008) 4000–4006.
[141] Q.H. Liu, G.M. Grim, A.B. Papandrew, A. Turhan, T.A. Zawodzinski, M.M. Mench, J. Electrochem. Soc. 159 (2012) A1246–A1252.
[142] J. Newman, J. Electrochem. Soc. 142 (1995) 97–101.
[143] M. Sankir, Y.S. Kim, B.S. Pivovar, J.E. Mcgrath, J. Memb. Sci. 299 (2007) 8–18.
[144] A. Roy, M.A. Hickner, B.R. Einsla, W.L. Harrison, J.E. Mcgrath, J. Polym. Sci. A 47 (2009) 384–391.
[145] K.T. Cho, P. Ridgway, A.Z. Weber, S. Haussener, V. Battaglia, V. Srinivasan, J. Electrochem. Soc. 159 (2012) A1806–A1815.
[146] H.Q. Zhu, Y.M. Zhang, L. Yue, W.S. Li, G.L. Li, D. Shu, H.Y. Chen, J. Power Sourc. 184 (2008) 637–640.
[147] M. Mermoux, Y. Chabre, A. Rousseau, Carbon 29 (1991) 469–474.
[148] H.Y. He, T. Riedl, A. Lerf, J. Klinowski, J. Phys. Chem. 100 (1996) 19954–19958.
[149] F.Y. Ban, S.R. Majid, N.M. Huang, H.N. Lim, Int. J. Electrochem. Sci. 7 (2012) 4345–4351.
[150] P. Han, H. Wang, Z. Liu, X. Chen, W. Ma, J. Yao, Y. Zhu, G. Cui, Carbon 49 (2011) 693–700.
[151] B. Fang, Y. Wei, T. Arai, S. Iwasa, M. Kumagai, J. Appl. Electrochem. 33 (2003) 197–203.
[152] S. Zhong, C. Padeste, M. Skyllas-Kazacos, J. Power Sourc. 45 (1993) 29–41.
[153] S. Zhong, M. Skyllas-Kazacos, J. Power Sourc. 39 (1992) 1–9.
[154] J. Maruyama, T. Hasegawa, S. Iwasaki, T. Fukuhara, M. Nogami, J. Electrochem. Soc. 160 (2013) A1293–A1298.
[155] H. Liu, T. Cai, Q. Song, L. Yang, Q. Xu, C. Yan, Int. J. Electrochem. Sci. 8 (2013) 2515–2523.
[156] M. Lopez-Atalaya, G. Codina, J.R. Perez, J.L. Vazquez, A. Aldaz, M.A. Climent, J. Power Sourc. 35 (1991) 225–234.
[157] H.S. Lim, A.M. Lackner, R.C. Knechtli, J. Electrochem. Soc. 124 (1977) 1154–1157.
[158] A.H. Whitehead, M. Harrer, J. Power Sourc. 230 (2013) 271–276.
[159] K.H. An, K.K. Jeon, W.S. Kim, Y.S. Park, S.C. Lim, D.J. Bae, J. Kor. Phys. Soc. 39 (2001) S511–S517.
[160] G. Girishkumar, K. Vinodgopal, P.V. Kamat, J. Phys. Chem. B 108 (2004) 19960–19966.
[161] K.S. Novoselov, A.K. Geim, S.V. Morozov, D. Jiang, Y. Zhang, S.V. Dubonos, I.V. Grigorieva, A.A. Firsov, Science 306 (2004) 666–669.
[162] M.H. Chakrabarti, C.T.J. Low, N.P. Brandon, V. Yufit, M.A. Hashim, M.F. Irfan, J. Akhtar, E. Ruiz-Trejo, M.A. Hussain, Electrochim. Acta 107 (2013) 425–440.
[163] C.T.J. Low, F.C. Walsh, M.H. Chakrabarti, M.A. Hashim, M.A. Hussain, Carbon 54 (2013) 1–21.
[164] K.E. Toghill, R.G. Compton, Int. J. Electrochem. Sci. 5 (2010) 1246–1301.
[165] A.K. Geim, K.S. Novoselov, Nat. Mater. 6 (2007) 183–191.
[166] D. Chen, L. Tang, J. Li, Chem. Soc. Rev. 39 (2010) 3157–3180.
[167] Y. Wang, Z. Shi, Y. Huang, Y. Ma, C. Wang, M. Chen, Y. Chen, J. Phys. Chem. C 113 (2009) 13103–13107.
[168] E.J. Yoo, J. Kim, E. Hosono, H.S. Zhou, T. Kudo, I. Honma, Nano Lett. 8 (2008) 2277–2282.
[169] L. Qu, Y.J. Baek, L. Dai, ACS Nano 4 (2010) 1321–1326.
[170] D. Vairavapandian, P. Vichchulada, M.D. Lay, Anal. Chim. Acta 626 (2008) 119–129.
[171] J. Chen, Y. Liu, A.I. Minett, C. Lynam, J. Wang, G.G. Wallace, Chem. Mater. 19 (2007) 3595–3597.
[172] D.T. Welna, L.T. Qu, B.E. Taylor, L.M. Dai, M.F. Durstock, J. Power Sourc. 196 (2011) 1455–1460.

[173] Y. Xing, L. Li, C.C. Chusuei, R.V. Hull, Langmuir 21 (2005) 4185–4190.
[174] A. Mohana Reddy, N. Rajalakshmi, S. Ramaprabhu, Carbon 46 (2008) 2–11.
[175] K.S. Hazra, N.A. Koratkar, D.S. Misra, Carbon 49 (2011) 4760–4766.
[176] W. Li, J. Liu, C. Yan, Carbon 49 (2011) 3463–3470.
[177] X. Rui, A. Parasuraman, W. Liu, D.H. Sim, Q. Yan, T.M. Lim, M. Skyllas-Kazacos, Carbon 64 (2013) 464–471.
[178] C. Lee, X. Wei, J.W. Kysar, J. Hone, Science 321 (2008) 385–388.
[179] A.A. Balandin, S. Ghosh, W. Bao, I. Calizo, D. Teweldebrhan, F. Miao, C.N. Lau, Nano Lett. 8 (2008) 902–907.
[180] K.I. Bolotin, K.J. Sikes, Z. Jiang, M. Klima, G. Fudenberg, J. Hone, P. Kim, H.L. Stormer, Solid State Commun. 146 (2008) 351–355.
[181] M.D. Stoller, S. Park, Y. Zhu, J. An, R.S. Ruoff, Nano Lett. 8 (2008) 3498–3502.
[182] P.J. Tsai, T.C. Chiu, P.H. Tsai, K.L. Lin, K.S. Lin, S.L.I. Chan, Int. J. Hydrogen Energy 37 (2012) 3491–3499.
[183] K.L. Huang, X.G. Li, S.Q. Liu, N. Tan, L.Q. Chen, Renew. Energy 33 (2008) 186–192.
[184] D. Scamman, G. Reade, E. Roberts, J. Power Sourc. 189 (2009) 1231–1239.
[185] S. Maldonado, S. Morin, K.J. Stevenson, Carbon 44 (2006) 1429–1437.
[186] R.A. Sidik, A.B. Anderson, N.P. Subramanian, S.P. Kumaraguru, B.N. Popov, J. Phys. Chem. B 110 (2006) 1787–1793.
[187] Y.Y. Shao, J.H. Sui, G.P. Yin, Y.Z. Gao, Appl. Catal. B Environ. 79 (2008) 89–99.
[188] G. Wu, D.Y. Li, C.S. Dai, D.L. Wang, N. Li, Langmuir 24 (2008) 3566–3575.
[189] K.P. Gong, F. Du, Z.H. Xia, M. Durstock, L.M. Dai, Science 323 (2009) 760–764.
[190] M.S. Saha, R.Y. Li, X.L. Sun, S.Y. Ye, Electrochem. Commun. 11 (2009) 438–441.
[191] L.P. Shi, Q.M. Gao, Y.H. Wu, Electroanalysis 21 (2009) 715–722.
[192] P.X. Han, Y.H. Yue, Z.H. Liu, W. Xu, L.X. Zhang, H.X. Xu, S. Dong, G. Cui, Energy Environ. Sci. 4 (2011) 4710–4717.
[193] J. Friedl, C.M. Bauer, A. Rinaldi, U. Stimming, Carbon 63 (2013) 228–239.
[194] C. Flox, M. Skoumal, J. Rubio-Garcia, T. Andreu, J.R. Morante, Appl. Energy 109 (2013) 344–351.
[195] D. Johnson, M. Reid, J. Electrochem. Soc. 132 (1985) 1058–1062.
[196] G. Codina, J.R. Perez, M. Lopez-Atalaya, J.L. Vazquez, A. Aldaz, J. Power Sourc. 48 (1994) 293–302.
[197] M. Lopez-Atalaya, G. Codina, J.R. Perez, J.L. Vazquez, A. Aldaz, J. Power Sourc. 39 (1992) 147–154.
[198] C.H. Bae, E.P.L. Roberts, R.A.W. Dryfe, Electrochim. Acta 48 (2002) 279–287.
[199] R. Savinell, C. Liu, R. Galasco, S. Chiang, J. Coetzee, J. Electrochem. Soc. 126 (1979) 357–360.
[200] C. Liu, R. Galasco, R. Savinell, J. Electrochem. Soc. 128 (1981) 1755–1757.
[201] C. Liu, R. Galasco, R. Savinell, J. Electrochem. Soc. 129 (1982) 2502–2505.
[202] Y. Wang, Y. Lin, C. Wan, J. Power Sourc. 13 (1984) 65–74.
[203] S. Langlois, F. Coeuret, J. Appl. Electrochem. 19 (1989) 43–50.
[204] M. Skyllas-Kazacos, G. Kazacos, G. Poon, H. Verseema, Int. J. Energy. Res. 34 (2010) 182–189.
[205] F. Xue, Y. Wang, W. Wang, X. Wang, Electrochim. Acta 53 (2008) 6636–6642.
[206] B. Fang, S. Iwasa, Y. Wei, T. Arai, M. Kumagai, Electrochim. Acta 47 (2002) 3971–3976.
[207] X. Xia, L. Tao, Y. Liu, J. Electrochem. Soc. 149 (2002) A426–A430.
[208] Y. Wen, J. Cheng, P. Ma, Y. Yang, Electrochim. Acta 53 (2008) 3514–3522.
[209] Y. Wen, J. Cheng, Y. Xun, P. Ma, Y.S. Yang, Electrochim. Acta 53 (2008) 6018–6023.
[210] Q. Liu, A.E.S. Sleightholme, A.A. Shinkle, Y. Li, L.T. Thompson, Electrochem. Commun. 11 (2009) 2312–2315.
[211] P. Lex, B. Jonshagen, Power Eng. J. 13 (1999) 142–148.
[212] K. Hasegawa, A. Kimura, T. Yamamura, Y. Shiokawa, J. Phys. Chem. Solid 66 (2005) 593–595.
[213] T. Yamamura, N. Watanabe, Y. Shiokawa, J. Alloys Compd. 408 (2006) 1260–1266.
[214] C.H. Bae, E.P.L. Roberts, M.H. Chakrabarti, M. Saleem, Int. J. Green Energy 8 (2011) 248–264.
[215] S.C. Chieng, M. Kazacos, M. Skyllas-Kazacos, J. Membr. Sci. 75 (1992) 81–91.
[216] Q. Liu, A.A. Shinkle, Y. Li, C.W. Monroe, L.T. Thompson, A.E.S. Sleightholme, Electrochem. Commun. 12 (2010) 1634–1637.
[217] A.E.S. Sleightholme, A.A. Shinkle, Q.H. Liu, Y.D. Li, C.W. Monroe, L.T. Thompson, J. Power Sourc. 196 (2011) 5742–5745.
[218] Y. Xu, Y. Wen, J. Cheng, G. Cao, Y. Yang, Electrochim. Acta 55 (2010) 715–720.
[219] M.H. Chakrabarti, R.A.W. Dryfe, E.P.L. Roberts, Electrochim. Acta 52 (2007) 2189–2195.
[220] M.H. Chakrabarti, E.P.L. Roberts, C.H. Bae, M. Saleem, Energy Convers. Manage. 52 (2011) 2501–2508.
[221] J. Mun, M.J. Lee, J.W. Park, D.J. Oh, D.Y. Lee, S.G. Doo, Electrochem. Solid State Lett. 15 (2012) A80–A82.
[222] Z. Li, S. Li, S. Liu, K. Huang, D. Fang, F. Wang, S. Peng, Electrochem. Solid State Lett. 14 (2011) A171–A173.
[223] L. Bahadori, N.S. Abdul-Manan, M.H. Chakrabarti, M.A. Hashim, F.S. Mjalli, I.M. AlNashef, M.A. Hussain, C.T.J. Low, Phys. Chem. Chem. Phys. 15 (2013) 1707–1714.
[224] D. Lloyd, T. Vainikka, K. Kontturi, Electrochim. Acta 100 (2013) 18–23.
[225] M.H. Chakrabarti, N.P. Brandon, M.A. Hashim, F.S. Mjalli, I.M. AlNashef, L. Bahadori, N.S.A. Manan, M.A. Hussain, V. Yufit, Int. J. Electrochem. Sci. 8 (2013) 9652–9676.
[226] M. Duduta, B. Ho, V.C. Wood, P. Limthongkul, V.E. Brunini, W.C. Carter, Y.-M. Chiang, Adv. Energy Mater. 1 (2011) 511–516.
[227] M.C. Tucker, V. Srinivasan, P.N. Ross, A.Z. Weber, J Appl. Electrochem. 43 (2013) 637–644.
[228] P. Simon, Y. Gogotsi, Acc. Chem. Res. 46 (2013) 1094–1103.
[229] J. Vatamanu, Z. Hu, D. Bedrov, C. Perez, Y. Gogotsi, J. Phys. Chem. Lett. 4 (2013) 2829–2837.
[230] J.-H. Kim, K.J. Kim, M.-S. Park, N.J. Lee, U. Hwang, H. Kim, Y.-J. Kim, Electrochem. Commun. 13 (2011) 997–1000.
[231] H.D. Pratt III, J.C. Leonard, L.A.M. Steele, C.L. Staiger, T.M. Anderson, Inorg. Chim. Acta 396 (2013) 78–83.
[232] H.D. Pratt III, A.J. Rose, C.L. Staiger, D. Ingersoll, T.M. Anderson, Dalton Trans. 40 (2011) 11396–11401.
[233] D. Zhang, Q. Liu, X. Shi, Y. Li, J. Power Sourc. 203 (2012) 201–205.
[234] M.H. Chakrabarti, F.S. Mjalli, I.M. AlNashef, M.A. Hashim, M.A. Hussain, L. Bahadori, C.T.J. Low, Renew. Sustain. Energy Rev. 30 (2014) 254–270.
[235] M.H. Chakrabarti, N.P. Brandon, F.S. Mjalli, L. Bahadori, I.M. AlNashef, M.A. Hashim, M.A. Hussain, C.T.J. Low, V. Yufit, J. Solution Chem. 42 (2013) 2329–2341.
[236] M. Moore, J. Watson, T.A. Zawodzinski, M. Zhang, R.M. Counce, ECS Trans. 41 (2012) 1–19.
[237] M. Gattrell, J. Qian, C. Stewart, P. Graham, B. MacDougall, Electrochim. Acta 51 (2005) 395–407.
[238] S.M. Shafeeyan, W.M.A.W. Daud, A. Houshmand, A. Arami-Niya, Appl. Surf. Sci. 257 (2011) 3936–3942.
[239] V. Yufit, B. Hale, M. Matian, P. Mazur, N.P. Brandon, J. Electrochem. Soc. 160 (2013) A856–A861.
[240] C. Menictas, M. Skyllas-Kazacos, J. Appl. Electrochem. 41 (2011) 1223–1232.
[241] N. Liu, F. Luo, H. Wu, Y. Liu, C. Zhang, J. Chen, Adv. Funct. Mater. 18 (2008) 1518–1525.
[242] J. Lu, J.X. Yang, J. Wang, A. Lim, S. Wang, K.P. Loh, ACS Nano 3 (2009) 2367–2375.
[243] A.A. Shinkle, A.E.S. Sleightholme, L.D. Griffith, L.T. Thompson, C.W. Monroe, J. Power Sourc. 206 (2012) 490–496.
[244] P.R. Shearing, L.E. Howard, P.S. Jørgensen, N.P. Brandon, S.J. Harris, Electrochem. Commun. 12 (2010) 374–377.
[245] N. Yoshizawa, O. Tanaike, H. Hatori, K. Yoshikawa, A. Kondo, T. Abe, Carbon 44 (2006) 2558–2564.
[246] I. Thorat, D. Stephenson, N. Zacharias, K. Zaghib, J. Harb, D. Wheeler, J. Power Sourc. 188 (2009) 592–600.
[247] M. Doyle, J. Newman, A. Gozdz, C. Schmutz, J.M. Tarascon, J. Electrochem. Soc. 143 (1996) 1890–1903.
[248] S.J. Cooper, M. Kishimoto, F. Tariq, R.S. Bradley, A.J. Marquis, N.P. Brandon, J.A. Kilner, P.R. Shearing, ECS Trans. 57 (2013) 2671–2678.
[249] F. Tariq, M. Kishimoto, S.J. Cooper, P.R. Shearing, N.P. Brandon, ECS Trans. 57 (2013) 2553–2562.
[250] H. Iwai, N. Shikazono, T. Matsui, H. Teshima, M. Kishimoto, R. Kishida, D. Hayashi, K. Matsuzaki, D. Kanno, M. Saito, H. Muroyama, K. Eguchi, N. Kasagi, H. Yoshida, J. Power Sourc. 195 (2010) 955–961.
[251] M. Kishimoto, H. Iwai, M. Saito, H. Yoshida, J. Power Sourc. 196 (2011) 4555–4563.
[252] P.R. Shearing, N.P. Brandon, J. Gelb, R. Bradley, P.J. Withers, A.J. Marquis, S. Cooper, S.J. Harris, J. Electrochem. Soc. 159 (2012) A1023–A1027.
[253] J.R. Izzo, A.S. Joshi, K.N. Grew, W.K.S. Chiu, A. Tkachuk, S.H. Wang, W.B. Yun, J. Electrochem. Soc. 155 (2008) B504–B508.
[254] P.R. Shearing, J.I. Golbert, R.J. Chater, N.P. Brandon, Chem. Eng. Sci. 64 (2009) 3928–3933.
[255] J.R. Wilson, W. Kobsiriphat, R. Mendoza, H.Y. Chen, J.M. Hiller, D.J. Miller, K. Thornton, P.W. Voorhees, S.B. Adler, S.A. Barnett, Nat. Mater. 5 (2006) 541–544.
[256] Y. Tian, A. Timmons, J.R. Dahn, J. Electrochem. Soc. 156 (2009) A187–A191.
[257] A. Sano, M. Kurihara, T. Abe, Z. Ogumi, J. Electrochem. Soc. 156 (2009) A639–A644.
[258] Y. Itou, Y. Ukyo, J. Power Sourc. 146 (2005) 39–44.
[259] J.R. Wilson, J.S. Cronin, S.A. Barnett, S.J. Harris, J. Power Sourc. 196 (2011) 3443–3447.
[260] F. Tariq, V. Yufit, M. Kishimoto, P.R. Shearing, S. Menkin, D. Golodnitsky, J. Gelb, E. Peled, N.P. Brandon, J. Power Sourc. 248 (2014) 1014–1020.
[261] V. Yufit, P. Shearing, R.W. Hamilton, P.D. Lee, M. Wu, N.P. Brandon, Electrochem. Commun. 13 (2011) 608–610.
[262] F. Tariq, R. Haswell, P.D. Lee, D.W. McComb, Acta Mater. 59 (2011) 2109–2120.
[263] G. Qiu, A.S. Joshi, C.R. Dennison, K.W. Knehr, E.C. Kumbur, Y. Sun, Electrochim. Acta 64 (2012) 46–64.
[264] G. Qiu, C.R. Dennison, K.W. Knehr, E.C. Kumbur, Y. Sun, J. Power Sourc. 219 (2012) 223–234.